iScience

Article

SNF1/AMPK controls its own localization by phosphorylating its activating kinase Sak1

Graphical abstract

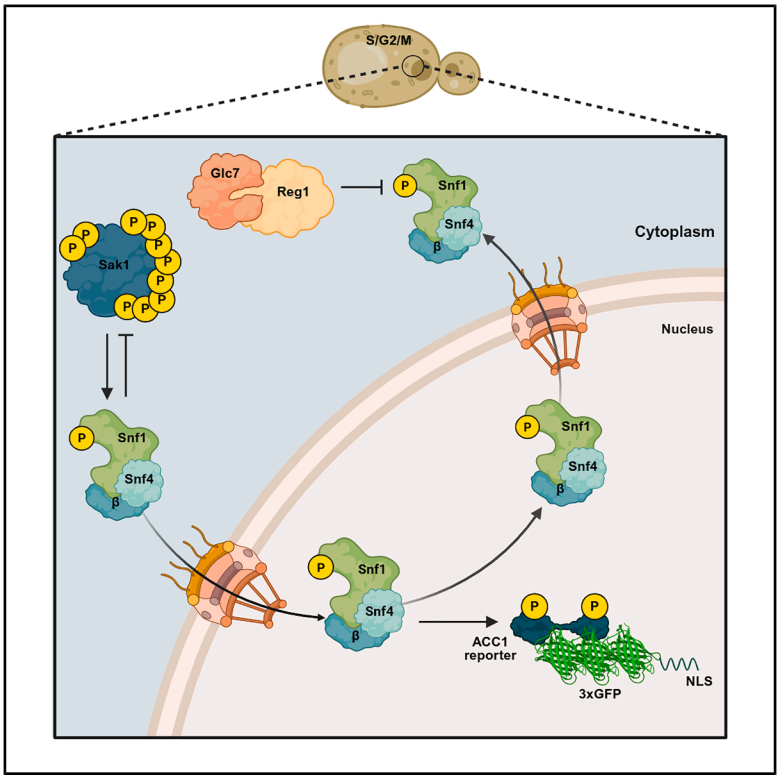

Authors

Hind Moukham, Marco Caligaris, Pauline Six, ..., Raffaele Nicastro, Farida Tripodi, Paola Coccetti

Correspondence

paola.coccetti@unimib.it

In brief

Molecular biology; Cell biology; Systems biology

Highlights

- SNF1 nuclear enrichment occurs mainly in S/G2/M cells upon glucose depletion
- SNF1 regulates its nuclear localization by phosphorylating the upstream kinase Sak1
- The non-phosphorylatable *sak1*^{10Ala} mutant exhibits a higher Snf1 nuclear entry
- Loss of Sak1 phosphorylation enhances nuclear SNF1 activity

Moukham et al., 2026, iScience *29*, 116357
July 17, 2026
https://doi.org/10.1016/j.isci.2026.116357

CellPress

iScience

CellPress
OPEN ACCESS

Article

SNF1/AMPK controls its own localization by phosphorylating its activating kinase Sak1

Hind Moukham,[1,7] Marco Caligaris,[2,5,7] Pauline Six,[2,6] Francesco Padovani,[3] Kurt M. Schmoller,[3] Claudio De Virgilio,[2] Raffaele Nicastro,[4] Farida Tripodi,[1,8] and Paola Coccetti[1,8,9,*]

[1]Department of Biotechnology and Biosciences, University of Milano-Bicocca, 20126 Milano, Italy
[2]Department of Biology, University of Fribourg, 1700 Fribourg, Switzerland
[3]Institute of Functional Epigenetics, Molecular Targets and Therapeutics Center, Helmholtz Zentrum München, Neuherberg, 85764 Munich, Germany
[4]Department of Biological Sciences, University of Limerick, V94 T9PX Limerick, Ireland
[5]Present address: Molecular and Cell Biology Laboratory, The Salk Institute for Biological Studies, 10010 N. Torrey Pines Road, La Jolla, CA 92037, USA
[6]Present address: Department for Visceral Surgery and Medicine, Inselspital, Bern University Hospital, University of Bern, Bern 3008, Switzerland
[7]These authors contributed equally
[8]Senior author
[9]Lead contact
*Correspondence: paola.coccetti@unimib.it
https://doi.org/10.1016/j.isci.2026.116357

SUMMARY

SNF1/AMPK is a key metabolic regulator in yeast, orchestrating cellular responses to glucose depletion. Its activation relies on phosphorylation of the α subunit by the upstream kinases Sak1, Tos3, and Elm1, with Sak1 as the primary regulator. Interestingly, ten Snf1-dependent phosphosites on Sak1 have been reported. Here, we explored Snf1 nuclear/cytoplasmic dynamics upon glucose depletion by using single-cell live imaging. Snf1 nuclear entry peaks rapidly after glucose depletion in a Sak1-dependent manner, before gradually decreasing over time. In the *sak1*^{10Ala} mutant, which cannot be phosphorylated by Snf1, Snf1 exhibits a higher nuclear entry compared to WT, predominantly in S/G2/M cells. Remarkably, this finding correlates with increased phosphorylation of the nuclear Snf1 reporter ACC1-3xGFP-NLS and results in better adaptation to glucose scarcity. Our findings highlight that Snf1 is able to regulate its own subcellular localization, which is critical for fine tuning its activity and downstream signaling during metabolic stress.

INTRODUCTION

In *Saccharomyces cerevisiae* the central component of the glucose repression pathway is the SNF1 kinase complex, an ortholog of the AMP-activated protein kinase complex (AMPK) in higher eukaryotes.[1] Similarly to AMPK, SNF1 acts to maintain energy homeostasis in conditions of energy limitation and, in yeast, it is specialized in the response to carbon stress, in particular to glucose scarcity. Indeed, by phosphorylating transcriptional repressors and activators (such as Mig1, Adr1, Cat8, and Sip4), SNF1 stimulates the expression of genes involved in respiration and gluconeogenesis and promotes the use of alternative carbon sources.[1,2] The SNF1 complex is a heterotrimeric complex constituted by one α catalytic subunit (Snf1) and two regulatory subunits, β (either Gal83, Sip1, or Sip2) and γ (Snf4).[3] Crucially, the structure of the complex, its subunits, and regulation are strongly conserved among all eukaryotes.[4,5]

The α catalytic subunit Snf1 presents a serine/threonine catalytic kinase domain (KD), bearing the activation loop (T-loop) and a conserved threonine residue (T210), and a regulatory domain (RD).[6] The RD contains an auto-inhibitory domain (AID) and a C-terminal domain (CTD) for the binding to the γ and β subunits.[7] The AID domain interacts with the Snf1 KD domain and Snf4 when cells are growing in high glucose, and the complex is poorly active. In low-glucose conditions, when SNF1 is active,[8,9] the binding between Snf1 and Snf4 prevents the inhibitory intramolecular interaction between the KD and AID domains.[10] The role of the three β subunits is connected to the control of the subcellular localization of the SNF1 complex: Sip1 triggers SNF1 recruitment at the vacuolar periphery, Sip2 is associated with SNF1 in the cytoplasm, and Gal83 determines SNF1 import into the nucleus.[11–13] Additionally, mitochondrial pools of SNF1 have been linked with the regulation of mitochondrial function and biogenesis.[14] The subcellular localization of SNF1 is dynamically modulated in response to metabolic changes.[15]

The activity of SNF1 is mainly controlled by the balance between the rates of phosphorylation and dephosphorylation of the T-loop on T210. SNF1 phosphorylation is mediated by three upstream kinases, called SNF1-activating kinases (SAKs): Sak1, Tos3, and Elm1, which are closely related to the mammalian LKB1 and CaMKK2.[16] The triple *sak1Δtos3Δelm1Δ* mutant displays a *snf1Δ*-like phenotype, exhibiting an inability to grow on

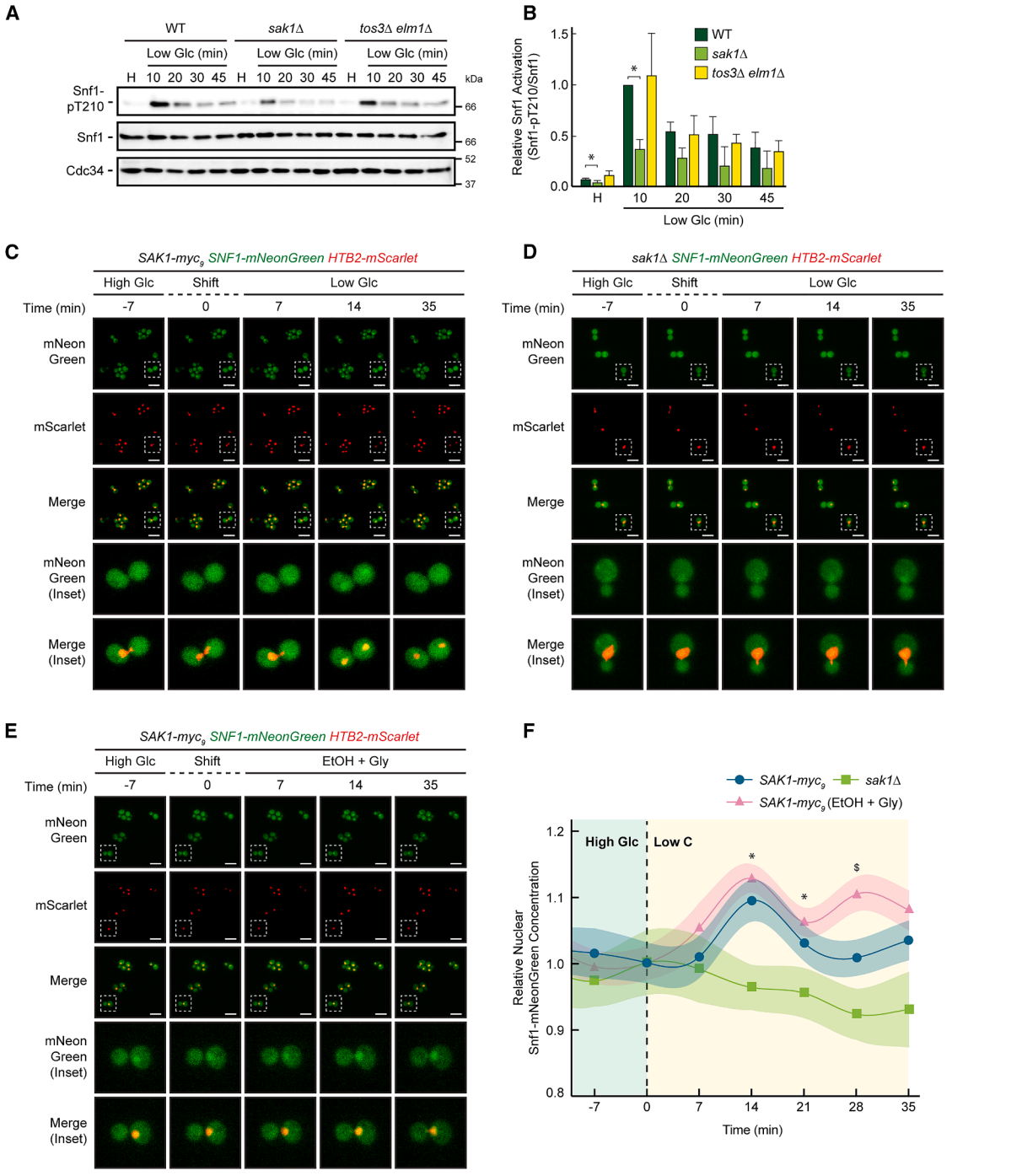

Figure 1. Sak1 is required for Snf1 phosphorylation and nuclear translocation upon glucose depletion. See also Figure S1

(A) Wild type, *sak1Δ*, and *tos3Δelm1Δ* strains were grown exponentially in high glucose (2%) medium and then shifted to low glucose (0.05%) medium. Whole-cell extracts were prepared at the indicated time points after the shift. Snf1 phosphorylation on T210 was detected by western blot using a phospho-specific anti-AMPK-pT172 antibody. Total Snf1 was detected using an anti-His_6 antibody. Cdc34 was probed as a loading control.

(B) The mean Snf1 phosphorylation level (Snf1-pT210/Snf1) was quantified and shown in the bar diagram ($n = 4$; +SD; unpaired Student's *t* test, $^*p \leq 0.05$).

(C–E) Wild type (*sak1Δ SAK1-myc9*) and *sak1Δ* strains expressing Snf1-mNeonGreen and the nuclear marker Htb2-mScarlet were grown exponentially in high glucose (2%) medium and shifted at time 0 to low glucose (0.05%; C, WT and D, *sak1Δ*), or to a medium containing 2% ethanol +3% glycerol (E, WT). Live-cell time-lapse imaging was performed using single-plane acquisition every 7 min following the shift. Representative images of mNeonGreen and mScarlet fluorescence, and enlarged cells (insets), are shown for the indicated time points ($n = 2$; scale bars, 10 μm).

(legend continued on next page)

carbon sources alternative to glucose and a failure to express *SUC2*, which encodes the enzyme invertase, in de-repressed conditions. In this mutant, Snf1 is not phosphorylated on T210 and thus is completely inactive. On the contrary, deleting two of the three kinases fails to cause any strong *snf1Δ*-related phenotype, indicating their functional redundancy.[16] Among the three upstream kinases, Sak1 is the primary SAK and it is the only kinase stably found in complex with Snf1, independently of glucose availability.[17,18] Conversely, SNF1 inactivation is dependent on T210 dephosphorylation by its main phosphatase Glc7, associated with its regulatory subunit Reg1, which together constitute the PP1/Reg1 (or Glc7/Reg1) phosphatase complex.[19] This modulation does not depend on a different activity of the upstream kinases, since the three SAKs are active toward T210 regardless of glucose concentration, both *in vitro* and *in vivo*.[16,20] On the contrary, Glc7/Reg1-dependent dephosphorylation of Snf1 is 10-fold slower in glucose-limited conditions. Interestingly, this does not depend on changes in the activity of Glc7/Reg1 itself, but rather on the accessibility of T210 to Glc7/Reg1, which varies according to glucose availability.[20] This could depend on the binding of Snf1 to the first glycolytic intermediate glucose-6-phosphate (Glc-6-P), since a mutant lacking the hexokinases cannot be dephosphorylated in response to glucose.[21]

Apart from being involved in metabolic regulation, SNF1/AMPK also regulates many other cellular processes, from stress response to DNA damage response, cell growth, and cell cycle. At the G1-to-S phase transition, SNF1 contributes to the expression of the G1 regulon to enter S phase,[22,23] while in mitosis, SNF1 localizes to the bud neck and contributes to the alignment of the mitotic spindle along the mother-bud axis.[24] These findings support the idea that SNF1 could act as a conserved energy checkpoint to coordinate cell growth and cell cycle progression. In line with this data, several findings indicate that yeast metabolism is tightly coordinated with cell-cycle progression.[25] For instance, the level of several metabolites varies significantly through the cell division cycle[26] and a temporal segregation of biosynthetic activities throughout the cell cycle was suggested.[27] Importantly, these oscillations appear to be regulated not only by cell-cycle components such as Cdk1[26] but also by key metabolic signaling pathways, including SNF1, TORC1, and PKA,[28] at least in part by direct phosphorylation of metabolic enzymes.[29,30]

Here, we investigated the precise dynamics of SNF1 nuclear entry, including the timing, its dependence on specific upstream kinases, and its behavior in live cells. Strikingly, we show that SNF1 nuclear enrichment upon glucose depletion, predominantly observed in cells at the S/G2/M phases of the cell cycle, is limited by a negative feedback mechanism. This mechanism involves SNF1-dependent phosphorylation of its upstream kinase Sak1 at multiple residues, highlighting the complexity of the interplay between signaling effectors, their upstream activators, and the cell cycle.

RESULTS

Sak1 is the primary upstream kinase activating Snf1 in low glucose

Previous studies have established that Sak1 is the primary upstream kinase responsible for SNF1 activation through phosphorylation of its α subunit.[17,31] In our experiments, to assess the contribution of specific upstream kinases to Snf1 phosphorylation dynamics, we analyzed the Snf1 phosphorylation on T210 in wild type (WT), *sak1Δ*, and *tos3Δelm1Δ* yeast strains after a glucose shift-down (0.05%) (Figures 1A and 1B). Yeast cells were grown in 2% glucose medium until mid-logarithmic phase and then shifted to low glucose (0.05%). Protein samples were collected at various time points (0, 10, 20, 30, and 45 min) and subjected to western blot analysis. In the WT strain, Snf1-pT210 level increased rapidly following glucose depletion, peaking at 10 min and gradually decreasing afterward, consistent with a transient activation pattern of Snf1. In contrast, the *sak1Δ* strain, lacking the primary upstream kinase Sak1, exhibited a significant reduction in Snf1-pT210 throughout the time course, confirming a key role of Sak1 in promoting Snf1 phosphorylation upon glucose starvation. Upon glucose depletion, the *tos3Δelm1Δ* strain showed an increase in Snf1 phosphorylation similar to WT cells, suggesting that Sak1 alone is sufficient for the phosphorylation increase observed in WT. Collectively, these results confirm the role of Sak1 as the predominant kinase responsible for Snf1 activation upon glucose depletion, with Tos3 and Elm1 playing minor roles. This prompted us to further investigate whether feedback phosphorylation of Sak1 by Snf1 might modulate this activation process.

Snf1 rapidly translocates to the nucleus in response to glucose depletion in a Sak1-dependent manner

Previous studies demonstrated that Snf1 translocation to the nucleus is a hallmark of glucose depletion, and this process requires the activity of upstream kinases, particularly Sak1.[31] However, the precise dynamics of Snf1 nuclear entry and exit, especially at single-cell resolution in live cells, have not been characterized. To address this point, we performed live-cell time-lapse imaging on yeast cells expressing Snf1-mNeonGreen and Htb2-mScarlet, as a nuclear marker. We captured fluorescent images every 7 min following a glucose shift-down or a shift to medium containing ethanol and glycerol to track Snf1 nuclear translocation in real time (Figures 1C–1F). In WT cells, Snf1 fluorescence was initially distributed in both the cytoplasm and nucleus. Upon shift to low glucose, Snf1 fluorescence intensity in the nucleus increased, reaching a peak at 14 min post shift (+11% relative to baseline T0), before gradually decreasing, indicating a transient nuclear response to metabolic changes (Figures 1C–1F). In contrast, in a *sak1Δ* mutant Snf1 failed to efficiently enter the nucleus, confirming that Sak1 is required for Snf1 nuclear translocation upon

(F) Nuclear Snf1 signal was quantified in single cells across the entire population (both budded and unbudded cells) for each condition (WT low glucose, $n = 122$; *sak1Δ* low glucose, $n = 30$; WT in EtOH + Gly, $n = 116$). Values were normalized to time 0 (high glucose) and plotted as mean ± SEM. The vertical dashed line indicates the time of the nutritional shift. Low C indicates low glucose shift for (C) and (D), and EtOH + Gly shift for (E). Spline lines were applied to highlight the continuous temporal trend of SNF1 localization without implying direct measurements between intermediate time points. Statistical significance ($p \leq 0.05$; unpaired Student's *t* test) is indicated as: at time points 14 and 21 min (*) indicate statistically significant differences between *SAK1-myc*$_9$ expressing and *sak1Δ* cells, while at time point 28 min ($) indicates statistically significant differences of cells expressing *SAK1-myc*$_9$ between shift to 0.05% Glc and EtOH + Gly.

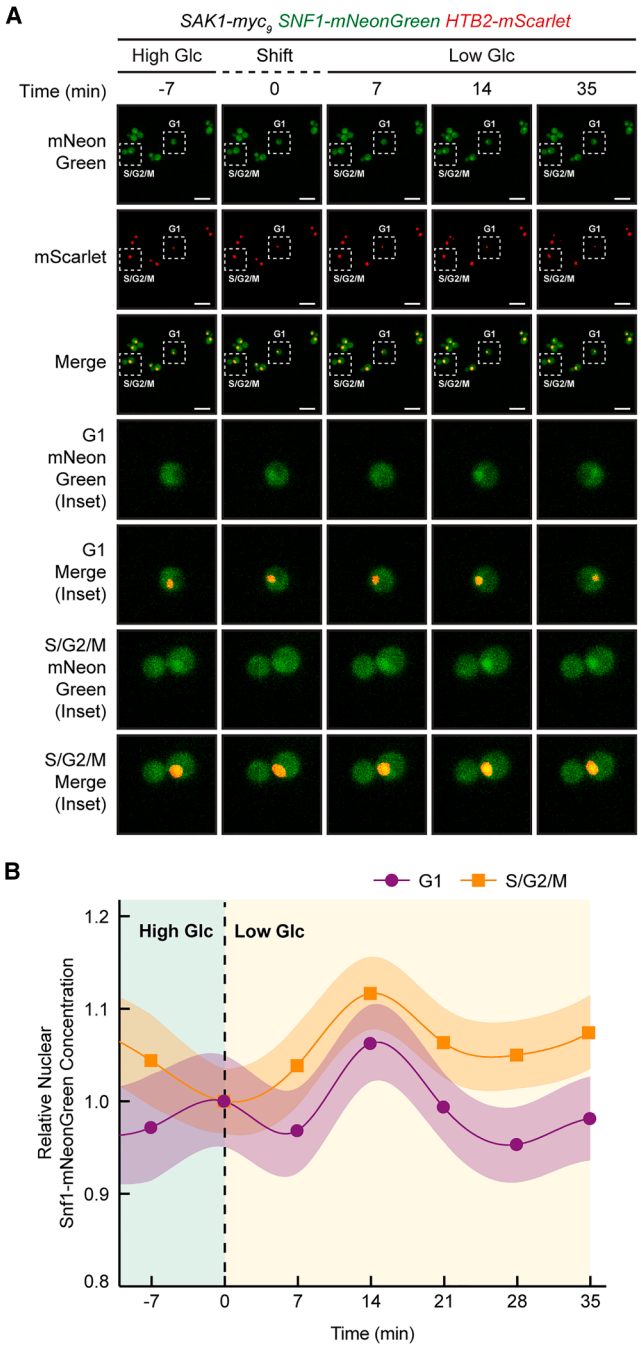

Figure 2. Snf1 nuclear translocation predominantly occurs in S/G2/M phase. See also Figure S2

(A) Wild-type (*sak1Δ SAK1-myc*$_9$) cells expressing Snf1-mNeonGreen and the nuclear marker Htb2-mScarlet were grown exponentially in high glucose (2%) medium and shifted at time 0 to low glucose (0.05%) medium. Live-cell time-lapse imaging was performed using single-plane acquisition every 7 min following the shift. Representative images of mNeonGreen and mScarlet fluorescence, and merged images with nuclear insets, are shown for the indicated time points. In addition, representative enlarged images from cells classified as G1 (unbudded) or S/G2/M (budded) are shown in the lower images (insets) (n = 2; scale bars, 10 μm).

(B) The nuclear Snf1-mNeonGreen concentration was quantified separately for G1 (n = 66) and S/G2/M phase cells (n = 71). Values were normalized relative to the mean nuclear intensity at time 0 (high glucose, set to 1.0) for each cell cycle phase, and plotted as mean ± SEM.

glucose depletion, as previously reported[31] (Figures 1D–1F). Although *SAK1* deletion alone completely abolishes the quick entry of SNF1 into the nucleus (Figures 1D–1F), due to the redundant roles of Tos3 and Elm1, *sak1Δ* cells are still viable if grown on media containing low glucose or alternative carbon sources[32,33] and in stress conditions,[34] demonstrating the substantial difference and independent relevance between rapid response to changing conditions and long-term adaptation.

In contrast to cells shifted to low glucose, cells shifted to a medium containing 2% ethanol and 3% glycerol exhibited a sustained nuclear Snf1 retention, with nuclear fluorescence reaching +14%, relative to baseline T0, and remaining elevated until 28 min (Figures 1E–1F). This may indicate that ethanol stress alters Snf1 regulation, possibly linking its localization to broader cellular stress responses rather than nutrient sensing alone. Nevertheless, we cannot exclude that sustained nuclear retention depends on a completely different rewiring of cellular metabolism in ethanol/glycerol condition. These observations led us to examine in more detail the dynamics of Snf1 nuclear localization following glucose depletion.

Snf1 nuclear translocation predominantly occurs in S/G2/M phase

Our analysis was performed with exponentially growing cells, which represent a mixed population of cells at various cell cycle stages. Given the prominent role of SNF1 in cell-cycle regulation,[23] and since metabolic activities oscillate throughout the cell cycle,[27] we investigated whether Snf1 nuclear localization might vary depending on the cell-cycle phase. Resolving this variability could help uncover subtle regulatory dynamics that are otherwise masked when averaging signals across heterogeneous populations. To address this aspect, based on bud morphology and nuclear marker segmentation, we categorized cells into G1 (unbudded) cells and S/G2/M (budded) phases, and measured Snf1 nuclear concentration over time within each group.

We observed that the nuclear concentration of Snf1 was higher in G1-phase cells compared to budded ones when studied under steady-state conditions in high glucose (Figure S1). This finding is consistent with the established role of the kinase in activating the G1 transcriptional program under high-glucose conditions.[23] After the shift to low glucose, a trend (not statistically significant) of higher nuclear accumulation of Snf1 was observed in S/G2/M-phase cells compared to G1-phase cells, both measured at the peak time point (14 min post-shift) and normalized to time 0, without reaching statistical significance (Figures 2A and 2B). This cell cycle-resolved analysis of Snf1 localization allowed us to detect informative trends that would have been missed in a bulk analysis.

SNF1 phosphorylates Sak1 to control its own activation and interaction

Previous phosphoproteomic studies in Caligaris et al.,[35] identified 10 SNF1-dependent phosphosites on Sak1. Furthermore,

earlier works had already suggested that SNF1 might phosphorylate Sak1.[17,18] Thus, to investigate the regulatory interplay between SNF1 and Sak1, we analyzed SNF1-dependent phosphorylation sites on Sak1. Strikingly, the phosphorylation levels of these sites were significantly reduced upon glucose shift-down when SNF1 activity was inhibited.[35] Notably, all these sites are located outside of the KD, with most located in the C terminus of the protein (Figure 3A), in agreement with the observations of Liu et al.[18]

To investigate whether these phosphosites are physiologically relevant, we generated a *sak1*^{10Ala} mutant, with Ser/Thr-to-Ala substitutions at the SNF1-controlled phosphosites, which did not exhibit any evident growth defect under both glucose repression and derepression conditions (Figure S2). Then, the Snf1-Sak1 interaction was evaluated in high glucose (2%) and 10 min after a glucose shift-down. Using co-immunoprecipitation assays, we confirmed a constitutive interaction between Snf1 and Sak1 in high glucose,[18] which remained unchanged upon shifting to low glucose medium in both strains (Figures 3B and 3C), suggesting that Sak1 phosphorylation does not affect the interaction.

To explore the functional role of these sites, the behavior of the *sak1*^{10Ala} mutant was analyzed in a shift down experiment, to assess the impact of SNF1-dependent Sak1 phosphorylation on the SNF1-signaling cascade. Western blot analysis and quantitative measurements (Figures 3D and 3E) revealed a significant difference in Snf1-T210 phosphorylation dynamics between the WT strain and the *sak1*^{10Ala} mutant upon shifting to low glucose conditions. In the WT strain, Snf1 phosphorylation on T210 peaked within 5 min, followed by a gradual decline, consistent with the transient phosphorylation pattern previously observed (Figures 1A and 1B). In contrast, the *sak1*^{10Ala} mutant exhibited elevated Snf1 phosphorylation at short time points, which persisted longer after the shift (Figures 3D and 3E). Remarkably, in the absence of the other two upstream kinases Tos3 and Elm1, the *sak1*^{10Ala} mutant exhibited a similar higher phosphorylation peak after the shift, while the sustained phosphorylation at longer time points was lost (Figures 3F and 3G), suggesting that the acute response completely depends on Sak1, while the sustained phosphorylation could be due to the presence of Tos3 and Elm1.

These results support the hypothesis that phosphorylation of Sak1 by SNF1 is required to limit maximal phosphorylation of Snf1 upon glucose shift-down. In the *sak1*^{10Ala} mutant, the lack of phosphorylatable sites on Sak1 prevents this negative feedback loop, leading to higher Snf1 phosphorylation, underscoring the importance of SNF1-mediated phosphorylation in fine-tuning cellular responses to metabolic stress that had not been systematically demonstrated before.

Loss of Sak1 phosphorylation increases Snf1 nuclear entry in S/G2/M

Since SNF1-dependent phosphorylation of Sak1 influences the extent and duration of Snf1 phosphorylation, we wondered whether Sak1 phosphorylation might also affect Snf1 nuclear localization. To investigate this, we performed live-cell time-lapse imaging of Snf1-mNeonGreen in yeast single cells expressing WT *SAK1* or the *sak1*^{10Ala} mutant. Before the glucose shift (time −7 min), Snf1-mNeonGreen fluorescence was distributed in both the cytoplasm and nucleus (Figures 4A and 4B). Following glucose depletion, a clear increase in nuclear fluorescence intensity was observed, indicating Snf1 translocation into the nucleus. Merging the green signal of Snf1-mNeonGreen with the red fluorescence of nuclear Htb2-mScarlet, Snf1 nuclear localization appeared as a yellow signal, confirming the nuclear localization of Snf1. This dynamic behavior was quantified in Figures 4C–4E. Interestingly, in *sak1*^{10Ala} cells, Snf1 nuclear localization in S/G2/M-phase cells was significantly higher than in G1-phase ones (24% vs. 3%, Figure 4C). Comparing the two strains, in G1-phase cells, both strains showed similar Snf1 nuclear dynamics (Figure 4D). In contrast, in S/G2/M-phase cells, Snf1 nuclear localization was higher in *sak1*^{10Ala} cells than in WT cells (Figure 4E). Together with our previous data, these findings reveal a coherent regulatory mechanism in which loss of Sak1 phosphorylation (in the *sak1*^{10Ala} mutant) leads to higher Snf1 phosphorylation, and enhanced nuclear accumulation of Snf1 in S/G2/M (budded) cells. These observations suggest that Sak1 phosphorylation serves as a key regulatory node controlling SNF1-signaling dynamics.

Sak1 phosphorylation modulates SNF1-dependent regulation of the nuclear ACC1 reporter

To complement our findings on Snf1 nuclear localization and activation dynamics, we analyzed nuclear SNF1 activity in WT and *sak1*^{10Ala} mutant strains. A synthetic reporter of SNF1 activity, ACC1-GFP (Figure 5A; scheme on the left), was previously developed.[36] This reporter, which we genomically integrated as a single copy, contains 13 amino acids of rat acetyl-CoA carboxylase ACC1, including the AMPK-targeted S79, with both a GFP and an HA tag.[37] Yeast SNF1 can recognize and phosphorylate S79 in ACC1, enabling us to monitor *in vivo* SNF1 activity by probing ACC1-GFP phosphorylation via western blot.[35,36,38] Since this reporter localizes to both the cytosol and nucleus (Figure 5B**)**, we initially fused a nuclear localization signal (NLS) to its C terminus (creating ACC1-GFP-NLS, Figure 5A; scheme in the middle) to promote nuclear enrichment and specifically monitor nuclear SNF1 activity. However, besides in the nucleus, this reporter was still observable in the cytosol (Figure 5B**)**. To overcome this issue, we increased the size of the reporter by adding two extra GFP copies (creating ACC1-3xGFP-NLS, Figure 5A; scheme on the right). This larger construct effectively reduced nuclear-cytosolic diffusion, increasing the nuclear-localized fraction (Figure 5B). To validate that the ACC1-3xGFP-NLS construct was phosphorylated in a SNF1-dependent manner, it was expressed in a *snf1Δ* strain. As expected, no detectable phosphorylation was observed in the *snf1Δ* strain, in contrast to WT cells (Figure 5C**)**.

Given the increased Snf1 nuclear entry observed in the *sak1*^{10Ala} mutant, we decided to analyze ACC1-S79 phosphorylation under glucose shift-down conditions using the nuclear ACC1-3xGFP-NLS reporter (Figures 5D and 5E). To enrich the S/G2/M population, we performed the shift-down from YPD medium culture (in which budded cells are the vast majority, around 85%) to low glucose medium. Western blot analysis revealed a transient increase in ACC1-S79 phosphorylation in the WT strain, peaking at 5 min after the shift and gradually decreasing over

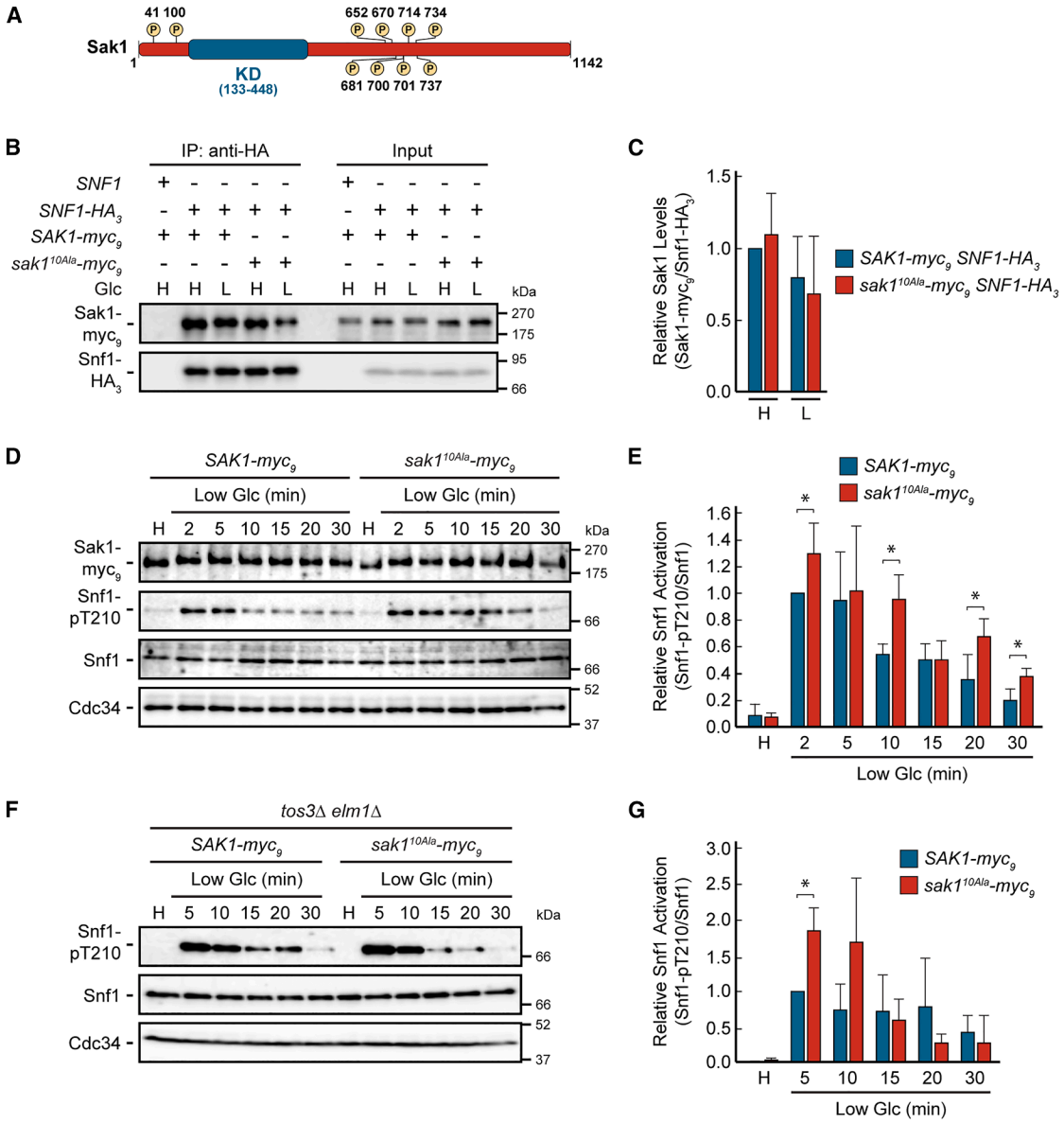

Figure 3. SNF1-mediated phosphorylation of Sak1 causes increased Snf1 phosphorylation

(A) Schematic illustration of Sak1, with the specific SNF1-dependent phosphorylation sites identified by Caligaris et al., 2023[35] (KD; kinase domain).

(B) *sak1Δ* cells expressing *SAK1-myc*$_9$ (WT) or *sak1*^{10Ala}-*myc*$_9$ (10Ala) and co-expressing Snf1-HA$_3$ were grown exponentially in high glucose medium (H) and then shifted to low glucose medium (L) for 10 min. Lysates (input) and anti-HA immunoprecipitates (IP: anti-HA) were analyzed by western blotting with anti-HA and anti-myc antibodies. A strain expressing *SAK1-myc*$_9$ and Snf1 (without a tag) was used as a negative control.

(C) Relative ratio between Sak1-myc$_9$ variants and Snf1-HA in coimmunoprecipitation assays shown in (B) (n = 5; +SD).

(D) Wild-type (*sak1Δ SAK1-myc*$_9$) and *sak1*^{10Ala}-*myc*$_9$ (*sak1Δ sak1*^{10Ala}-*myc*$_9$) strains were grown exponentially in high glucose (2%) medium and shifted to low glucose (0.05%) medium at time 0. Whole cell extracts were prepared at the indicated time points after the shift (0, 2, 5, 10, 15, 20, and 30 min). Snf1 phosphorylation on T210 was detected by western blot using a phospho-specific anti-AMPK-pT172 antibody. Total Snf1 was detected using an anti-His$_6$ antibody. Sak1-myc$_9$ and Cdc34 were probed as controls.

(E) The mean Snf1 phosphorylation level (Snf1-pT210/Snf1) was quantified and shown in the bar diagram (n = 5; +SD; unpaired Student's t test, $^*p \leq 0.05$).

(F) *tos3Δelm1Δsak1Δ* cells expressing either *SAK1-myc*$_9$ or *sak1*^{10Ala}-*myc*$_9$ were grown exponentially in high glucose (2%) medium and shifted to low glucose (0.05%) medium at time 0. Whole cell extracts were prepared at the indicated time points after the shift (0, 5, 10, 15, 20, and 30 min). Snf1 phosphorylation on T210 was detected by western blot using a phospho-specific anti-AMPK-pT172 antibody. Total Snf1 was detected using an anti-His$_6$ antibody. Sak1-myc$_9$ and Cdc34 were probed as controls.

(G) The mean Snf1 phosphorylation level (Snf1-pT210/Snf1) was quantified and shown in the bar diagram (n = 5; +SD; unpaired Student's t test, $^*p \leq 0.05$).

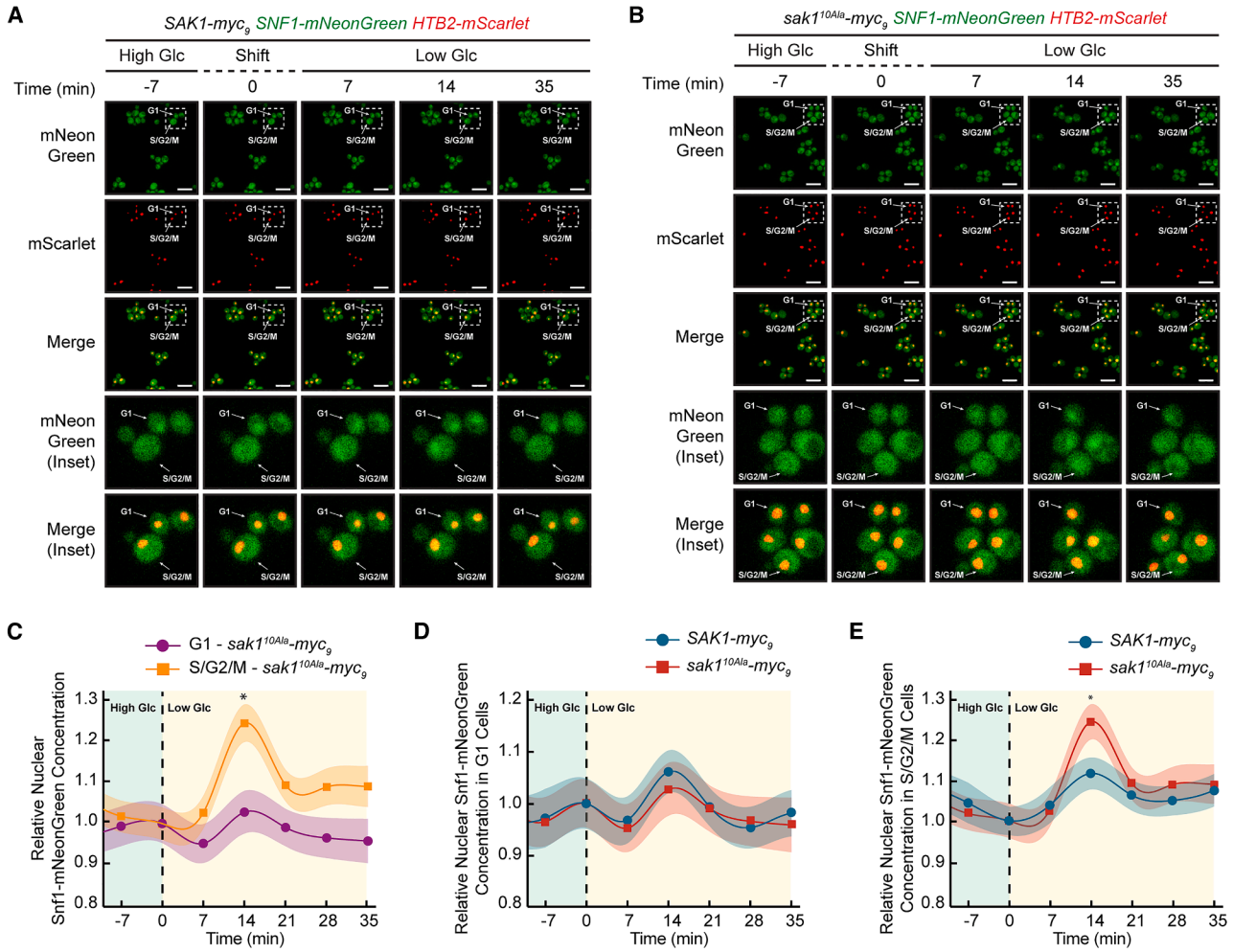

Figure 4. Loss of Sak1 phosphorylation increases Snf1 nuclear accumulation in S/G2/M-phase cells

(A and B) Wild type (*sak1Δ SAK1-myc*$_9$) (A) or *sak1*^{10Ala}*-myc*$_9$ (*sak1Δ sak1*^{10Ala}*-myc*$_9$) (B) strains expressing Snf1-mNeonGreen and the nuclear marker Htb2-mScarlet were grown exponentially in high glucose (2%) medium and shifted at time 0 to low glucose (0.05%) medium. Live-cell time-lapse imaging was performed using single-plane acquisition every 7 min following the shift. Representative images of mNeonGreen and mScarlet fluorescence are shown for the indicated time points. Representative nuclei from G1-phase (unbudded) and S/G2/M-phase (budded) cells are shown in the inset panels ($n = 2$; scale bars, 10 μm).

(C) The nuclear Snf1-mNeonGreen concentration in the *sak1*^{10Ala}*-myc*$_9$ (*sak1Δ sak1*^{10Ala}*-myc*$_9$) strain was quantified separately for G1 ($n = 77$) and S/G2/M phase cells ($n = 70$). Values were normalized relative to the mean nuclear intensity at time 0 (high glucose, set to 1.0) for each cell cycle phase, and plotted as mean ± SEM (unpaired Student's *t* test, $^*p \leq 0.05$).

(D and E) The nuclear Snf1-mNeonGreen concentration was quantified separately for G1-phase (WT $n = 66$, *sak1*^{10Ala} $n = 70$) (C) and S/G2/M-phase cells (WT $n = 70$, *sak1*^{10Ala} $n = 77$) (D). Values were normalized relative to the mean nuclear concentration at time 0 (high glucose) for each cell cycle phase and plotted as mean ± SEM (unpaired Student's *t* test, $^*p \leq 0.05$).

time, following the same trend as Snf1-T210 phosphorylation and activation (Figure 3B**)**. In contrast, the *sak1*^{10Ala} strain exhibited higher levels of ACC1-S79 phosphorylation, particularly at the 5-min time point. This suggests higher Snf1 accumulation in the mutant, in agreement with the higher Snf1 nuclear localization reported in Figures 4A and 4C. The levels of the total reporter remained stable across all time points, confirming that the observed changes in ACC1-S79 phosphorylation were not due to differences in protein abundance or loading.

Under the same conditions, we measured the level of *SUC2* mRNA, a typical SNF1-dependent transcript, in high glucose and 10 min after the shift to low glucose. A significantly higher expression of *SUC2* was observed in the *sak1*^{10Ala} mutant after the shift compared to the WT (Figure 5F), consistent with the phosphorylation of the nuclear ACC1-reporter. These results further support the model in which loss of feedback regulation on Sak1 leads to sustained Snf1 phosphorylation and nuclear accumulation, resulting in enhanced phosphorylation of nuclear substrates.

To evaluate the phenotypic impact caused by these differences in the *sak1*^{10Ala} strain, cell growth after the shift to low glucose was monitored. Interestingly, cell growth was significantly slower in the *sak1*^{10Ala} mutant compared to the WT (Figure 5G). This was associated with the mutant's inability to

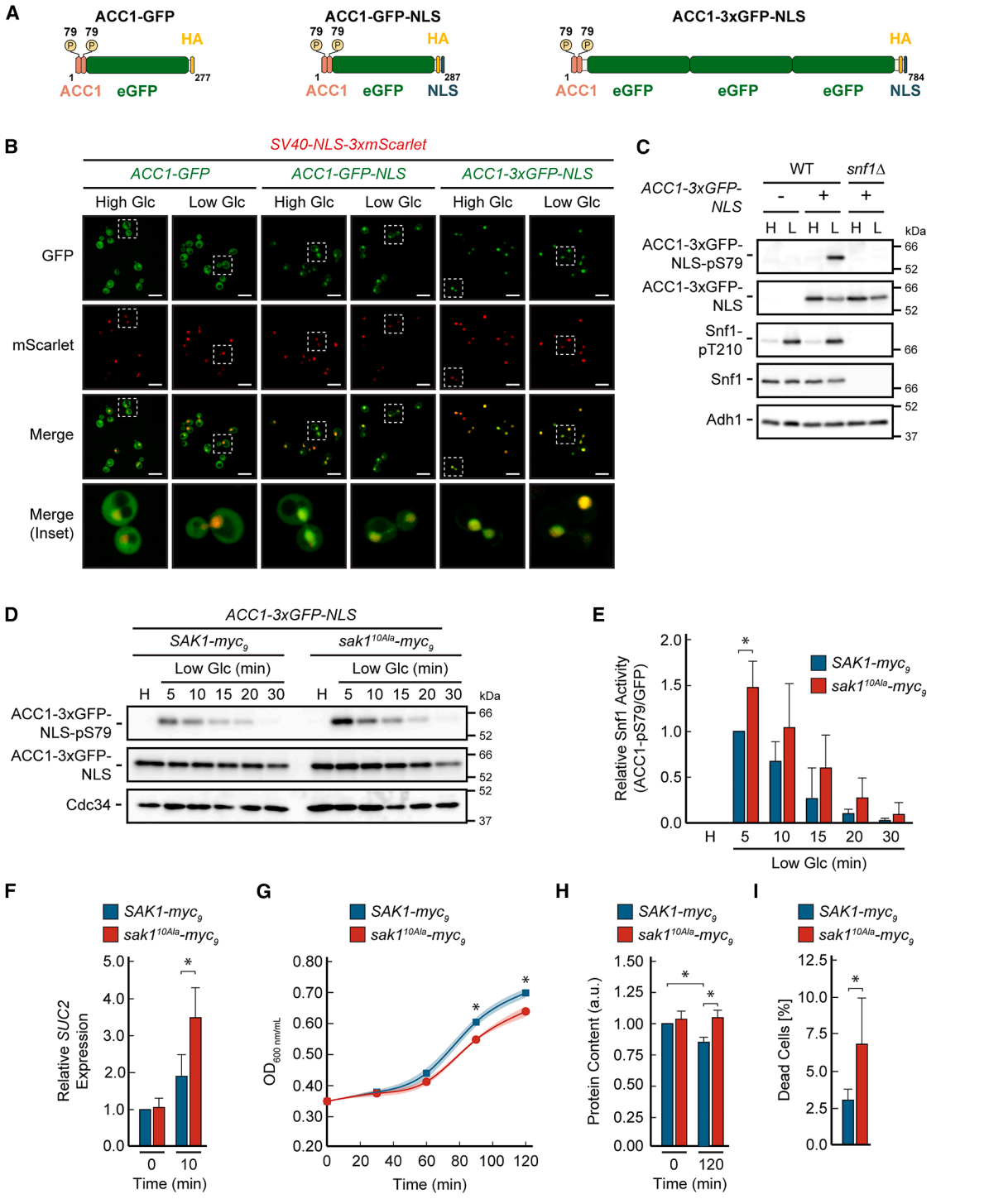

Figure 5. Loss of Sak1 phosphorylation enhances nuclear SNF1 activity

(A) Schematic illustrations of ACC1-GFP, ACC1-GFP-NLS, and ACC1-3xGFP-NLS. Each construct contains 13 amino acids of rat ACC1 in tandem, eGFP, and HA, as described in Deroover et al.[36] The nuclear localization signal (NLS) was added to target the reporter to the nucleus, while the 3×GFP variant was included to increase the reporter's size and enhance its nuclear retention.

(B) Wild-type strains expressing ACC1-GFP, ACC1-GFP-NLS, or ACC1-3xGFP-NLS and the nuclear marker SV40-NLS-3xmScarlet were grown exponentially in high glucose (2%) medium and shifted to low glucose (0.05%) medium for 10 min. Representative images of GFP and mScarlet fluorescence, and merged images with nuclear insets, are shown (n = 3; scale bars, 10 μm).

(legend continued on next page)

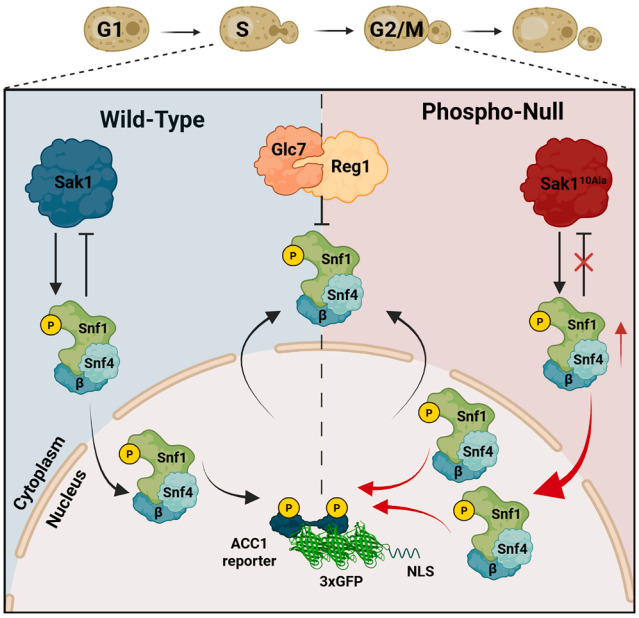

Figure 6. Schematic representation of the feedback regulation of Snf1 activation and nuclear localization

In wild-type cells Sak1 phosphorylation on Snf1 promotes SNF1 entry into the nucleus, thus increasing SNF1 nuclear activity upon glucose shift down. In the phospho-null *sak1*^{10Ala} mutant strain, the loss of Snf1 phosphorylation on Sak1 leads to a higher Snf1 phosphorylation following glucose shift-down, thus leading to a higher SNF1 nuclear level and consequently to an increased SNF1 nuclear activity, especially in S-G2-M-cells. Created with BioRender.com.

reset the total protein content in low glucose (Figure 5H), ultimately resulting in more than 2-fold increase in cell death 24 h after the shift (Figure 5I). These data suggest that the increased SNF1 nuclear activation of the *sak1*^{10Ala} mutant is detrimental to the overall fitness of the population following glucose reduction.

DISCUSSION

All cells must coordinate metabolism, cell growth, and cell cycle with nutrient availability to guarantee viability also during environmental changes. While SNF1/AMPK has long been recognized as a master regulator of metabolic adaptation to glucose scarcity,[5] the fine modulation of its activation dynamics and spatial distribution remains only partially understood both in yeast[39] and in more complex multicellular eukaryotes.[40,41] In this multilayered regulatory system, the first, and most studied, level of SNF1 regulation is represented by Snf1 phosphorylation on T210. In addition, the subcellular localization of the SNF1 complex, which is regulated by the association with the three alternative β subunits, determines its spatially different activity.[11,12,39] Other studies have more recently described levels of modulation involving Snf1 sumoylation,[42] regulation by pH through its poly-His tract,[43] and sensing of glucose availability through Glc-6-P.[44]

Here, we add a new level of regulation to this intricate picture, demonstrating that SNF1 establishes a new dynamic negative feedback mechanism by phosphorylating Sak1 on multiple sites, outside its KD. Previous findings established that Sak1 is the primary SAK.[16,17,31] However, its activity has long been considered constitutive, with most of the regulation being attributed to the changes in the dephosphorylation rate of T210 by the phosphatase Glc7/Reg1.[3,19] Nevertheless, phosphorylation of Sak1 by SNF1 was suggested almost 20 years ago in yeast,[17,18] and confirmed recently by our phosphoproteomics data which pinpointed the phosphorylated sites.[35] Here, we demonstrate that a negative feedback modulates the ability of Sak1 to promote T210 phosphorylation of Snf1 and regulates Snf1 nuclear accumulation upon glucose scarcity, a function required for adaptation to nutritional fluctuations but irrelevant in steady-state conditions (Figure S2) (Figure 6). Indeed, when SNF1 cannot phosphorylate and inhibit Sak1, Snf1 is hyperphosphorylated and shows higher nuclear localization upon glucose withdrawal, particularly in S/G2/M-phase cells (Figures 3D and 3E; Figure 4). This leads to increased nuclear SNF1 activity, indicating that feedback phosphorylation of Sak1 acts as a regulatory constraint that limits the extent of SNF1 nuclear signaling, important to adapt to the new nutritional condition and maintain the overall fitness of the population (Figures 5 and 6). In keeping with our data, cells lacking the two Snf1 phosphatases Reg1 and Sit4 are inviable,[45] indicating that excessive SNF1 activation is detrimental for cell viability. Interestingly, the Glc7-Reg1 phosphatase complex, which inactivates SNF1, has been predominantly localized to the cytoplasm,[46] suggesting that nuclear

(C) Wild-type (WT) or *snf1Δ* cells expressing the *ACC1-3xGFP-NLS* reporter were grown exponentially in high glucose (H) and then shifted to low glucose medium (L) for 15 min. Phosphorylation of the *bona fide* SNF1 target residue S79 in ACC1-3xGFP-NLS and of T210 in Snf1 was detected by western blot analyses of whole cell extracts using phospho-specific antibodies against the respective phospho-residues. Anti-GFP and anti-His_6 antibodies were used to detect the levels of ACC1-3xGFP-NLS and Snf1, respectively. Anti-Adh1 antibody was used to probe Adh1 and served as a loading control.

(D) Wild-type (*sak1Δ SAK1-myc*$_9$) and *sak1*^{10Ala}*-myc*$_9$ (*sak1Δ sak1*^{10Ala}*-myc*$_9$) strains expressing the nuclear ACC1-NLS-3xGFP reporter were grown exponentially in YPD medium (85%–88% budded cells) and shifted at time 0 to low glucose (0.05%) medium. Whole cell extracts were prepared at the indicated time points after the shift. Phosphorylation of ACC1 (S79) was detected by western blot using a phospho-specific anti-ACC1-pS79 antibody. Total ACC1-NLS-3xGFP levels were detected using an anti-GFP antibody. Cdc34 was probed as a loading control.

(E) The mean SNF1 activity toward the ACC1 reporter (ACC1-pS79/GFP) was quantified (n = 4; +SD; unpaired Student's t test, *$p \leq 0.05$).

(F) Wild-type (*sak1Δ SAK1-myc*$_9$) and *sak1*^{10Ala}*-myc*$_9$ (*sak1Δ sak1*^{10Ala}*-myc*$_9$) strains were grown exponentially in YPD medium and shifted at time 0 to low glucose (0.05%) medium. mRNAs were prepared at 0 and 10 min after the shift. Relative expression levels of the *SUC2* gene is shown in the bar diagram (n = 3; +SD; unpaired Student's t test, *$p \leq 0.05$).

(G) Wild-type (*sak1Δ SAK1-myc*$_9$) and *sak1*^{10Ala}*-myc*$_9$ (*sak1Δ sak1*^{10Ala}*-myc*$_9$) strains were grown exponentially in YPD medium and shifted at time 0 to low glucose (0.05%) medium. Cell growth was monitored over time (n = 3, +SD; unpaired Student's t test, *$p \leq 0.05$).

(H) Wild-type (*sak1Δ SAK1-myc*$_9$) and *sak1*^{10Ala}*-myc*$_9$ (*sak1Δ sak1*^{10Ala}*-myc*$_9$) strains were grown exponentially in YPD medium and shifted at time 0 to low glucose (0.05%) medium. Protein cell content was measured at 0 and 120 min after the shift (n = 4, +SD; unpaired Student's t test, *$p \leq 0.05$).

(I) Cell death of the cells in (G) was assessed 24 h after the shift by propidium iodide staining (n = 5–6; +SD; unpaired Student's t test, *$p \leq 0.05$).

SNF1 may be relatively protected from rapid dephosphorylation. Accordingly, the enhanced nuclear accumulation observed in the *sak1*^{10Ala} mutant may result from both increased entry and prolonged nuclear retention of phosphorylated SNF1. One of the most unexpected findings is that Snf1 nuclear dynamics are modulated across the cell cycle. Notably, only a limited fraction of Snf1 translocates to the nucleus upon glucose depletion, and this nuclear accumulation is highly dynamic and transient (Figures 1C–1F). The stronger nuclear accumulation of Snf1 observed in S/G2/M-phase cells may reflect a higher biosynthetic demand of these phases, when SNF1-driven reprogramming of gene expression and metabolism is particularly needed. Recent findings have suggested a potential temporal segregation of biosynthetic activities throughout the cell cycle[27] and that these oscillations might be influenced by changes of major metabolic signaling pathways.[28] Within this framework, the differential activation of the Sak1-SNF1 circuit in S/G2/M may reflect a physiological adaptation to the distinct metabolic requirement of these cell-cycle phases. Nevertheless, many other possible mechanisms could explain the observed cell-cycle difference in Snf1 localization, such as changes in β subunit composition, cell-cycle modulation of nuclear transport, or specific regulations of phosphatases.

Interestingly, we previously reported that active SNF1 is localized at the division site from the time of bud emergence to cytokinesis.[24] Remarkably, under steady-state conditions in high glucose, the nuclear concentration of Snf1 is higher during the G1 phase than in the S/G2/M phases in both WT and *sak1*^{10Ala} cells, although the difference is more pronounced in WT cells (Figure S1). This observation aligns with the previously reported role of nuclear SNF1 in promoting the transcription of G1-phase genes[23] and suggests that the loss of negative feedback may influence the regulation of the G1/S transition also under high-glucose conditions. Therefore, we propose that the mechanism described here may play a role in the precise coordination of nutrient sensing, metabolism, and cell-cycle progression, thereby mitigating excessive transcriptional responses during transient nutritional fluctuations.

Negative feedback mechanisms are widely used in signaling cascades to maintain cellular homeostasis and adapt to environmental changes.[47,48] In budding yeast, such mechanisms are well documented in the regulation of the cAMP/PKA pathway,[49] the TORC1 pathway,[50,51] and the MAPK pathway.[52,53] As concerns the AMPK pathway, a feedback mechanism has been reported in *Arabidopsis thaliana*, where activated SnRK1.1 can phosphorylate its upstream kinases GRIK1 and GRIK2, reducing their catalytic activity and thereby limiting further SnRK1.1 activation.[54] Similarly, in higher eukaryotes AMPK phosphorylates multiple residues of one of its upstream kinases, CaMKK2, downregulating its autonomous function while leaving its calcium-activated activity unaffected.[55] To further complicate this intricate regulatory system, AMPK-activating kinases can undergo auto-phosphorylation, acting as a positive feedback mechanism to enhance their own activity, both in plants[54] and in mammalian cells.[56,57] The presence of conserved feedback loops across species underscores the remarkable complexity of SNF1/AMPK regulation, a network whose full dynamics remain elusive. Our findings on the SNF1 negative feedback provide critical mechanistic insights, helping to clarify key aspects of the regulatory network of AMPK-dependent kinases.

Limitations of the study

This study, while providing a clear molecular description of the Sak1-SNF1 feedback regulation, has some limitations. A key limitation is the unresolved mechanistic link between Snf1 nuclear localization and the cell-cycle phase. While we suggest that phase-specific metabolic requirements may contribute to this behavior, this hypothesis remains to be experimentally validated and represents an opportunity for future studies. Moreover, our study examined the response to glucose reduction, leaving open the question of how alternative nutritional stresses might differentially influence Snf1 dynamics.

RESOURCE AVAILABILITY

Lead contact

Further information and requests for resources and reagents should be directed to and will be fulfilled by the lead contact, Paola Coccetti (paola.coccetti@unimib.it).

Materials availability

All materials will be made available upon request.

Data and code availability

- All data reported in this paper will be shared by the lead contact upon request.
- This paper does not report original code.
- Any additional information required to reanalyze the data reported in this paper is available from the lead contact upon request.

ACKNOWLEDGMENTS

We thank Marie-Pierre Péli-Gulli for the constructive discussions. Malika Jaquenoud, Susanne Stumpe, Olga Sudan, and Stefano Busti for technical assistance. Graphical images were created with BioRender.com and published with permission. This research was supported by grants from the Italian Ministry of University and Research (MUR) 2024-ATE-031 (to P.C.), 2023-ATE-0068 (to F.T.), and the Swiss National Science Foundation (184671 to C.D.V.). This work was also supported by the Helmholtz Association (to K.M.S.) and the Canton of Fribourg (to C.D.V.).

AUTHOR CONTRIBUTIONS

Conceptualization and writing – original draft, H.M., F.T., and P.C.; methodology, F.P.; investigation, formal analysis, data curation, and visualization, H.M., M.C., F.T., and P.S.; funding acquisition, P.C., F.T., C.D.V., and K.M.S.; writing – review and editing, K.M.S., F.P., C.D.V., and R.N.; supervision, P.C., F.T., and K.M.S.

DECLARATION OF INTERESTS

The authors declare no competing interests.

STAR★METHODS

Detailed methods are provided in the online version of this paper and include the following:

- KEY RESOURCES TABLE
- EXPERIMENTAL MODEL AND STUDY PARTICIPANT DETAILS
- METHOD DETAILS
  - Cytofluorimetric analyses
  - Live cell imaging microscopy and microfluidics experimental setup

- Quantitative analysis and cell cycle analysis
- Western blot analysis
- ACC1-3xGFP-NLS reporter assay
- Co-immunoprecipitation (Co-IP) assay

- QUANTIFICATION AND STATISTICAL ANALYSIS

SUPPLEMENTAL INFORMATION

Supplemental information can be found online at https://doi.org/10.1016/j.isci.2026.116357.

Received: November 11, 2025
Revised: May 6, 2026
Accepted: May 27, 2026

REFERENCES

1. Hedbacker, K., and Carlson, M. (2008). SNF1/AMPK pathways in yeast. Front. Biosci. *13*, 2408–2420. https://doi.org/10.2741/2854.
2. Coccetti, P., Nicastro, R., and Tripodi, F. (2018). Conventional and emerging roles of the energy sensor Snf1/AMPK in Saccharomyces cerevisiae. Microb. Cell *5*, 482–494. https://doi.org/10.15698/mic2018.11.655.
3. Sanz, P., Viana, R., and Garcia-Gimeno, M.A. (2016). AMPK in Yeast: The SNF1 (Sucrose Non-fermenting 1) Protein Kinase Complex. Exp. Suppl., 353–353374. https://doi.org/10.1007/978-3-319-43589-3_14.
4. Hardie, D.G. (2007). AMP-activated/SNF1 protein kinases: conserved guardians of cellular energy. Nat. Rev. Mol. Cell Biol. *8*, 774–785. https://doi.org/10.1038/nrm2249.
5. Crozet, P., Margalha, L., Confraria, A., Rodrigues, A., Martinho, C., Adamo, M., Elias, C.A., and Baena-González, E. (2014). Mechanisms of regulation of SNF1/AMPK/SnRK1 protein kinases. Front. Plant Sci. *5*, 190. https://doi.org/10.3389/fpls.2014.00190.
6. McCartney, R.R., Rubenstein, E.M., and Schmidt, M.C. (2005). Snf1 kinase complexes with different beta subunits display stress-dependent preferences for the three Snf1-activating kinases. Curr. Genet. *47*, 335–344. https://doi.org/10.1007/s00294-005-0576-2.
7. Crute, B.E., Seefeld, K., Gamble, J., Kemp, B.E., and Witters, L.A. (1998). Functional domains of the alpha1 catalytic subunit of the AMP-activated protein kinase. J. Biol. Chem. *273*, 35347–35354. https://doi.org/10.1074/jbc.273.52.35347.
8. Chen, L., Jiao, Z.-H., Zheng, L.-S., Zhang, Y.-Y., Xie, S.-T., Wang, Z.-X., and Wu, J.-W. (2009). Structural insight into the autoinhibition mechanism of AMP-activated protein kinase. Nature *459*, 1146–1149. https://doi.org/10.1038/nature08075.
9. Jiang, R., and Carlson, M. (1996). Glucose regulates protein interactions within the yeast SNF1 protein kinase complex. Genes Dev. *10*, 3105–3115. https://doi.org/10.1101/gad.10.24.3105.
10. Leech, A., Nath, N., McCartney, R.R., and Schmidt, M.C. (2003). Isolation of mutations in the catalytic domain of the snf1 kinase that render its activity independent of the snf4 subunit. Eukaryot. Cell *2*, 265–273. https://doi.org/10.1128/EC.2.2.265-273.2003.
11. Vincent, O., Townley, R., Kuchin, S., and Carlson, M. (2001). Subcellular localization of the Snf1 kinase is regulated by specific beta subunits and a novel glucose signaling mechanism. Genes Dev. *15*, 1104–1114. https://doi.org/10.1101/gad.879301.
12. Mangat, S., Chandrashekarappa, D., McCartney, R.R., Elbing, K., and Schmidt, M.C. (2010). Differential roles of the glycogen-binding domains of beta subunits in regulation of the Snf1 kinase complex. Eukaryot. Cell *9*, 173–183. https://doi.org/10.1128/EC.00267-09.
13. Hedbacker, K., Townley, R., and Carlson, M. (2004). Cyclic AMP-dependent protein kinase regulates the subcellular localization of Snf1-Sip1 protein kinase. Mol. Cell Biol. *24*, 1836–1843. https://doi.org/10.1128/MCB.24.5.1836-1843.2004.
14. Kayikci, Ö., and Nielsen, J. (2015). Glucose repression in Saccharomyces cerevisiae. FEMS Yeast Res. *15*, fov068. https://doi.org/10.1093/femsyr/fov068.
15. Braam, S., Tripodi, F., Österberg, L., Persson, S., Welkenhuysen, N., Coccetti, P., and Cvijovic, M. (2024). Exploring carbon source related localization and phosphorylation in the Snf1/Mig1 network using population and single cell-based approaches. Microb. Cell *11*, 143–154. https://doi.org/10.15698/mic2024.05.822.
16. Hong, S.-P., Leiper, F.C., Woods, A., Carling, D., and Carlson, M. (2003). Activation of yeast Snf1 and mammalian AMP-activated protein kinase by upstream kinases. Proc. Natl. Acad. Sci. USA *100*, 8839–8843. https://doi.org/10.1073/pnas.1533136100.
17. Elbing, K., McCartney, R.R., and Schmidt, M.C. (2006). Purification and characterization of the three Snf1-activating kinases of Saccharomyces cerevisiae. Biochem. J. *393*, 797–805. https://doi.org/10.1042/BJ20051213.
18. Liu, Y., Xu, X., and Carlson, M. (2011). Interaction of SNF1 protein kinase with its activating kinase Sak1. Eukaryot. Cell *10*, 313–319. https://doi.org/10.1128/EC.00291-10.
19. McCartney, R.R., and Schmidt, M.C. (2001). Regulation of Snf1 kinase. Activation requires phosphorylation of threonine 210 by an upstream kinase as well as a distinct step mediated by the Snf4 subunit. J. Biol. Chem. *276*, 36460–36466. https://doi.org/10.1074/jbc.M104418200.
20. Rubenstein, E.M., McCartney, R.R., Zhang, C., Shokat, K.M., Shirra, M.K., Arndt, K.M., and Schmidt, M.C. (2008). Access denied: Snf1 activation loop phosphorylation is controlled by availability of the phosphorylated threonine 210 to the PP1 phosphatase. J. Biol. Chem. *283*, 222–230. https://doi.org/10.1074/jbc.M707957200.
21. Milanesi, R., Coccetti, P., and Tripodi, F. (2020). The Regulatory Role of Key Metabolites in the Control of Cell Signaling. Biomolecules *10*, 862. https://doi.org/10.3390/biom10060862.
22. Pessina, S., Tsiarentsyeva, V., Busnelli, S., Vanoni, M., Alberghina, L., and Coccetti, P. (2010). Snf1/AMPK promotes S-phase entrance by controlling CLB5 transcription in budding yeast. Cell Cycle Georget. Tex *9*, 2189–2200. https://doi.org/10.4161/cc.9.11.11847.
23. Busnelli, S., Tripodi, F., Nicastro, R., Cirulli, C., Tedeschi, G., Pagliarin, R., Alberghina, L., and Coccetti, P. (2013). Snf1/AMPK promotes SBF and MBF-dependent transcription in budding yeast. Biochim. Biophys. Acta *1833*, 3254–3264. https://doi.org/10.1016/j.bbamcr.2013.09.014.
24. Tripodi, F., Fraschini, R., Zocchi, M., Reghellin, V., and Coccetti, P. (2018). Snf1/AMPK is involved in the mitotic spindle alignment in Saccharomyces cerevisiae. Sci. Rep. *8*, 5853. https://doi.org/10.1038/s41598-018-24252-y.
25. Ewald, J.C. (2018). How yeast coordinates metabolism, growth and division. Curr. Opin. Microbiol. *45*, 1–7. https://doi.org/10.1016/j.mib.2017.12.012.
26. Ewald, J.C., Kuehne, A., Zamboni, N., and Skotheim, J.M. (2016). The Yeast Cyclin-Dependent Kinase Routes Carbon Fluxes to Fuel Cell Cycle Progression. Mol. Cell *62*, 532–545. https://doi.org/10.1016/j.molcel.2016.02.017.
27. Takhaveev, V., Özsezen, S., Smith, E.N., Zylstra, A., Chaillet, M.L., Chen, H., Papagiannakis, A., Milias-Argeitis, A., and Heinemann, M. (2023). Temporal segregation of biosynthetic processes is responsible for metabolic oscillations during the budding yeast cell cycle. Nat. Metab. *5*, 294–313. https://doi.org/10.1038/s42255-023-00741-x.
28. Guerra, P., Vuillemenot, L.-A.P.E., van Oppen, Y.B., Been, M., and Milias-Argeitis, A. (2022). TORC1 and PKA activity towards ribosome biogenesis oscillates in synchrony with the budding yeast cell cycle. J. Cell Sci. *135*, jcs260378. https://doi.org/10.1242/jcs.260378.
29. Zhang, L., Winkler, S., Schlottmann, F.P., Kohlbacher, O., Elias, J.E., Skotheim, J.M., and Ewald, J.C. (2019). Multiple Layers of Phospho-Regulation Coordinate Metabolism and the Cell Cycle in Budding Yeast. Front. Cell Dev. Biol. *7*, 338. https://doi.org/10.3389/fcell.2019.00338.
30. Tripodi, F., Nicastro, R., Reghellin, V., and Coccetti, P. (2015). Post-translational modifications on yeast carbon metabolism: Regulatory

mechanisms beyond transcriptional control. Biochim. Biophys. Acta *1850*, 620–627. https://doi.org/10.1016/j.bbagen.2014.12.010.

31. Hedbacker, K., Hong, S.-P., and Carlson, M. (2004). Pak1 protein kinase regulates activation and nuclear localization of Snf1-Gal83 protein kinase. Mol. Cell Biol. *24*, 8255–8263. https://doi.org/10.1128/MCB.24.18.8255-8263.2004.
32. Hong, S.-P., Momcilovic, M., and Carlson, M. (2005). Function of mammalian LKB1 and Ca2+/calmodulin-dependent protein kinase kinase alpha as Snf1-activating kinases in yeast. J. Biol. Chem. *280*, 21804–21809. https://doi.org/10.1074/jbc.M501887200.
33. Nath, N., McCartney, R.R., and Schmidt, M.C. (2003). Yeast Pak1 kinase associates with and activates Snf1. Mol. Cell Biol. *23*, 3909–3917. https://doi.org/10.1128/MCB.23.11.3909-3917.2003.
34. Hong, S.-P., and Carlson, M. (2007). Regulation of snf1 protein kinase in response to environmental stress. J. Biol. Chem. *282*, 16838–16845. https://doi.org/10.1074/jbc.M700146200.
35. Caligaris, M., Nicastro, R., Hu, Z., Tripodi, F., Hummel, J.E., Pillet, B., Deprez, M.-A., Winderickx, J., Rospert, S., Coccetti, P., et al. (2023). Snf1/AMPK fine-tunes TORC1 signaling in response to glucose starvation. eLife *12*, e84319. https://doi.org/10.7554/eLife.84319.
36. Deroover, S., Ghillebert, R., Broeckx, T., Winderickx, J., and Rolland, F. (2016). Trehalose-6-phosphate synthesis controls yeast gluconeogenesis downstream and independent of SNF1. FEMS Yeast Res. *16*, fow036. https://doi.org/10.1093/femsyr/fow036.
37. Dyck, J.R., Kudo, N., Barr, A.J., Davies, S.P., Hardie, D.G., and Lopaschuk, G.D. (1999). Phosphorylation control of cardiac acetyl-CoA carboxylase by cAMP-dependent protein kinase and 5'-AMP activated protein kinase. Eur. J. Biochem. *262*, 184–190. https://doi.org/10.1046/j.1432-1327.1999.00371.x.
38. Tripodi, F., Castoldi, A., Nicastro, R., Reghellin, V., Lombardi, L., Airoldi, C., Falletta, E., Maffioli, E., Scarcia, P., Palmieri, L., et al. (2018). Methionine supplementation stimulates mitochondrial respiration. Biochim. Biophys. Acta. Mol. Cell Res. *1865*, 1901–1913. https://doi.org/10.1016/j.bbamcr.2018.09.007.
39. Chandrashekarappa, D.G., McCartney, R.R., O'Donnell, A.F., and Schmidt, M.C. (2016). The β subunit of yeast AMP-activated protein kinase directs substrate specificity in response to alkaline stress. Cell. Signal. *28*, 1881–1893. https://doi.org/10.1016/j.cellsig.2016.08.016.
40. Chauhan, A.S., Zhuang, L., and Gan, B. (2020). Spatial control of AMPK signaling at subcellular compartments. Crit. Rev. Biochem. Mol. Biol. *55*, 17–32. https://doi.org/10.1080/10409238.2020.1727840.
41. Schmitt, D.L., Curtis, S.D., Lyons, A.C., Zhang, J.-F., Chen, M., He, C.Y., Mehta, S., Shaw, R.J., and Zhang, J. (2022). Spatial regulation of AMPK signaling revealed by a sensitive kinase activity reporter. Nat. Commun. *13*, 3856. https://doi.org/10.1038/s41467-022-31190-x.
42. Simpson-Lavy, K.J., and Johnston, M. (2013). SUMOylation regulates the SNF1 protein kinase. Proc. Natl. Acad. Sci. USA *110*, 17432–17437. https://doi.org/10.1073/pnas.1304839110.
43. Simpson-Lavy, K.J., and Kupiec, M. (2022). Regulation of yeast Snf1 (AMPK) by a polyhistidine containing pH sensing module. iScience *25*, 105083. https://doi.org/10.1016/j.isci.2022.105083.
44. Milanesi, R., Tripodi, F., Vertemara, J., Tisi, R., and Coccetti, P. (2021). AMPK Phosphorylation Is Controlled by Glucose Transport Rate in a PKA-Independent Manner. Int. J. Mol. Sci. *22*, 9483. https://doi.org/10.3390/ijms22179483.
45. Ruiz, A., Xu, X., and Carlson, M. (2011). Roles of two protein phosphatases, Reg1-Glc7 and Sit4, and glycogen synthesis in regulation of SNF1 protein kinase. Proc. Natl. Acad. Sci. USA *108*, 6349–6354. https://doi.org/10.1073/pnas.1102758108.
46. Dombek, K.M., Voronkova, V., Raney, A., and Young, E.T. (1999). Functional analysis of the yeast Glc7-binding protein Reg1 identifies a protein phosphatase type 1-binding motif as essential for repression of ADH2 expression. Mol. Cell Biol. *19*, 6029–6040. https://doi.org/10.1128/MCB.19.9.6029.
47. Nguyen, L.K., and Kholodenko, B.N. (2016). Feedback regulation in cell signalling: Lessons for cancer therapeutics. Semin. Cell Dev. Biol. *50*, 85–94. https://doi.org/10.1016/j.semcdb.2015.09.024.
48. Brandman, O., and Meyer, T. (2008). Feedback loops shape cellular signals in space and time. Science *322*, 390–395. https://doi.org/10.1126/science.1160617.
49. Vandamme, J., Castermans, D., and Thevelein, J.M. (2012). Molecular mechanisms of feedback inhibition of protein kinase A on intracellular cAMP accumulation. Cell. Signal. *24*, 1610–1618. https://doi.org/10.1016/j.cellsig.2012.04.001.
50. Péli-Gulli, M.-P., Raucci, S., Hu, Z., Dengjel, J., and De Virgilio, C. (2017). Feedback Inhibition of the Rag GTPase GAP Complex Lst4-Lst7 Safeguards TORC1 from Hyperactivation by Amino Acid Signals. Cell Rep. *20*, 281–288. https://doi.org/10.1016/j.celrep.2017.06.058.
51. Nicastro, R., Péli-Gulli, M.-P., Caligaris, M., Jaquenoud, M., Dokládal, L., Alba, J., Tripodi, F., Pillet, B., Brunner, M., Stumpe, M., et al. (2025). TORC1 autonomously controls its spatial partitioning via the Rag GTPase tether Tco89. Cell Rep. *44*, 115683. https://doi.org/10.1016/j.celrep.2025.115683.
52. Hao, N., Zeng, Y., Elston, T.C., and Dohlman, H.G. (2008). Control of MAPK specificity by feedback phosphorylation of shared adaptor protein Ste50. J. Biol. Chem. *283*, 33798–33802. https://doi.org/10.1074/jbc.C800179200.
53. Hao, N., Behar, M., Parnell, S.C., Torres, M.P., Borchers, C.H., Elston, T.C., and Dohlman, H.G. (2007). A systems-biology analysis of feedback inhibition in the Sho1 osmotic-stress-response pathway. Curr. Biol. *17*, 659–667. https://doi.org/10.1016/j.cub.2007.02.044.
54. Crozet, P., Jammes, F., Valot, B., Ambard-Bretteville, F., Nessler, S., Hodges, M., Vidal, J., and Thomas, M. (2010). Cross-phosphorylation between Arabidopsis thaliana sucrose nonfermenting 1-related protein kinase 1 (AtSnRK1) and its activating kinase (AtSnAK) determines their catalytic activities. J. Biol. Chem. *285*, 12071–12077. https://doi.org/10.1074/jbc.M109.079194.
55. Nakanishi, A., Hatano, N., Fujiwara, Y., Sha'ri, A., Takabatake, S., Akano, H., Kanayama, N., Magari, M., Nozaki, N., and Tokumitsu, H. (2017). AMP-activated protein kinase-mediated feedback phosphorylation controls the Ca2+/calmodulin (CaM) dependence of Ca2+/CaM-dependent protein kinase kinase β. J. Biol. Chem. *292*, 19804–19813. https://doi.org/10.1074/jbc.M117.805085.
56. Boudeau, J., Baas, A.F., Deak, M., Morrice, N.A., Kieloch, A., Schutkowski, M., Prescott, A.R., Clevers, H.C., and Alessi, D.R. (2003). MO25alpha/beta interact with STRADalpha/beta enhancing their ability to bind, activate and localize LKB1 in the cytoplasm. EMBO J. *22*, 5102–5114. https://doi.org/10.1093/emboj/cdg490.
57. Tokumitsu, H., Hatano, N., Fujimoto, T., Yurimoto, S., and Kobayashi, R. (2011). Generation of autonomous activity of Ca(2+)/calmodulin-dependent protein kinase kinase β by autophosphorylation. Biochemistry *50*, 8193–8201. https://doi.org/10.1021/bi201005g.
58. Coccetti, P., Tripodi, F., Tedeschi, G., Nonnis, S., Marin, O., Fantinato, S., Cirulli, C., Vanoni, M., and Alberghina, L. (2008). The CK2 phosphorylation of the catalytic domain of Cdc34 modulates its activity at the G1 to S transition in *Saccharomyces cerevisiae*. Cell Cycle *7*, 1391–1401. https://doi.org/10.4161/cc.7.10.5825.
59. Binda, M., Péli-Gulli, M.P., Bonfils, G., Panchaud, N., Urban, J., Sturgill, T.W., Loewith, R., and De Virgilio, C. (2009). The Vam6 GEF controls TORC1 by activating the EGO complex. Mol. Cell *35*, 563–573. https://doi.org/10.1016/j.molcel.2009.06.033.
60. Sikorski, R.S., and Hieter, P. (1989). A system of shuttle vectors and yeast host strains designed for efficient manipulation of DNA in *Saccharomyces cerevisiae*. Genetics *122*, 19–27. https://doi.org/10.1093/genetics/122.1.19.

61. Christianson, T.W., Sikorski, R.S., Dante, M., Shero, J.H., and Hieter, P. (1992). Multifunctional yeast high-copy-number shuttle vectors. Gene *110*, 119–122. https://doi.org/10.1016/0378-1119(92)90454-W.

62. Caligaris, M., and De Virgilio, C. (2024). Proxies introduce bias in decoding TORC1 activity. MicroPubl. Biol. *2024*. https://doi.org/10.17912/micropub.biology.001170.

63. Longtine, M.S., McKenzie, A., 3rd, Demarini, D.J., Shah, N.G., Wach, A., Brachat, A., Philippsen, P., and Pringle, J.R. (1998). Additional modules for versatile and economical PCR-based gene deletion and modification in *Saccharomyces cerevisiae*. Yeast *14*, 953–961. https://doi.org/10.1002/(SICI)1097-0061(199807)14:10<953::AID-YEA293>3.0.CO;2-U.

64. Janke, C., Magiera, M.M., Rathfelder, N., Taxis, C., Reber, S., Maekawa, H., Moreno-Borchart, A., Doenges, G., Schwob, E., Schiebel, E., and Knop, M. (2004). A versatile toolbox for PCR-based tagging of yeast genes: new fluorescent proteins, more markers and promoter substitution cassettes. Yeast *21*, 947–962. https://doi.org/10.1002/yea.1142.

65. Wosika, V., Durandau, E., Varidel, C., Aymoz, D., Schmitt, M., and Pelet, S. (2016). New families of single integration vectors and gene tagging plasmids for genetic manipulations in budding yeast. Mol. Genet. Genomics. *291*, 2231–2240. https://doi.org/10.1007/s00438-016-1249-1.

66. Padovani, F., Mairhörmann, B., Falter-Braun, P., Lengefeld, J., and Schmoller, K.M. (2022). Segmentation, tracking and cell cycle analysis of live-cell imaging data with Cell-ACDC. BMC Biol. *20*, 174. https://doi.org/10.1186/s12915-022-01372-6.

67. Coccetti, P., Rossi, R.L., Sternieri, F., Porro, D., Russo, G.L., Di Fonzo, A., Magni, F., Vanoni, M., and Alberghina, L. (2004). Mutations of the CK2 phosphorylation site of Sic1 affect cell size and S-Cdk kinase activity in Saccharomyces cerevisiae. Mol. Microbiol. *51*, 447–460. https://doi.org/10.1046/j.1365-2958.2003.03836.x.

68. Dietler, N., Minder, M., Gligorovski, V., Economou, A.M., Joly, D.A.H.L., Sadeghi, A., Chan, C.H.M., Koziński, M., Weigert, M., Bitbol, A.-F., and Rahi, S.J. (2020). A convolutional neural network segments yeast microscopy images with high accuracy. Nat. Commun. *11*, 5723. https://doi.org/10.1038/s41467-020-19557-4.

69. Kukhtevich, I.V., Lohrberg, N., Padovani, F., Schneider, R., and Schmoller, K.M. (2020). Cell size sets the diameter of the budding yeast contractile ring. Nat. Commun. *11*, 2952. https://doi.org/10.1038/s41467-020-16764-x.

70. Bradford, M.M. (1976). A rapid and sensitive method for the quantitation of microgram quantities of protein utilizing the principle of protein-dye binding. Anal. Biochem. *72*, 248–254. https://doi.org/10.1016/0003-2697(76)90527-3.

STAR★METHODS

KEY RESOURCES TABLE

REAGENT or RESOURCE	SOURCE	IDENTIFIER
Antibodies		
Rabbit polyclonal anti-Adh1 (1:50′000)	Calbiochem	Cat# 126745-1 ML; RRID: AB_11214375
Mouse monoclonal anti-HA (12CA5) (1:1′000)	Roche	Cat# 11666606001; RRID: AB_514506
Mouse monoclonal anti-Myc-tag (9B11) (1:1′000)	Cell Signaling Technology	Cat# 2276, RRID: AB_331783
Mouse polyclonal anti-GFP (1:3′000)	Roche	Cat# 11814460001; RRID: AB_390913
Mouse monoclonal anti-poly-His (1:1′000)	Sigma-Aldrich	Cat# H1029; RRID: AB_260015
Rabbit polyclonal anti-ACC1-pSer79 (1:500)	Cell Signaling Technology	Cat# 3661; RRID: AB_330337
Rabbit polyclonal anti-AMPK-pThr172 (1:1′000)	Cell Signaling Technology	Cat# 2535; RRID: AB_331250
Rabbit polyclonal anti-Cdc34 (1:5′000)	Coccetti lab	Coccetti et al.[58]
Goat anti-mouse IgG-HRP conjugate (1:5′000)	Sigma-Aldrich	Cat# A9917; RRID: AB_258476
Goat anti-rabbit IgG-HRP conjugate (1:5′000)	Cell Signaling Technology	Cat# 7074; RRID: AB_2099233
Bacterial and virus strains		
E. coli DH5α	CGSC	12384
Chemicals, peptides, and recombinant proteins		
Yeast nitrogen base w/o amino acids	Formedium	CYN0410
D-Glucose monohydrate	Millipore	49159
Uracil	MP Biomedicals	103204
L-Leucine	MP Biomedicals	102158
L-Histidine	MP Biomedicals	101954
Anti-HA affinity matrix	Roche	11815016001
SDS	Sigma-Aldrich	75746
TCA	Sigma-Aldrich	27242
DTT	AppliChem	A1101
Urea	Sigma-Aldrich	33247
Tween 20	AppliChem	A4974
Trizma base	Sigma-Aldrich	T1503
PEG	Sigma-Aldrich	81240
Phusion polymerase	Thermo Scientific	F5302
Ammonium sulfate	MP Biomedicals	4808211
Complete EDTA-free Protease Inhibitor Cocktail	Roche	11-697-498-001
Drop-out Mix Synthetic, minus Ura w/o YNB	US Biological	D9535
YPD Broth	US Biological	Y2075
LB Broth (Lennox)	CONDA	1231
Pefabloc	Sigma-Aldrich	76307
PhosSTOP	Roche	04-906-837-001
KOD OneTM PCR Master Mix	TOYOBO	KMM-101
Glycerol	Sigma-Aldrich	49770
Nonidet P-40	AppliChem	A1694
Sodium chloride	Sigma-Aldrich	71380
Propidium iodide	Merck	81845
Fluorescein isothiocyanate (FITC)	Merck	46951

(*Continued on next page*)

Continued

REAGENT or RESOURCE	SOURCE	IDENTIFIER
Critical commercial assays		
ECL Western Blotting Detection	GE Healthcare	RPN2106
Radiance Plus Sensitive ECL	Azure Biosystems	AC2103
Microfluidic plates	Millipore	Y04C-02
Deposited data		
Raw Data	Mendeley Data Link	https://board.unimib.it/preview/kfppmjgdh9?a=d0f80df6-5a63-4708-9b13-71cd75bdb02c
Experimental models: Organisms/strains		
BY4741	Euroscarf	Mat a; his3Δ1 ura3Δ0 leu2Δ0 met15Δ0
YL515	Binda et al.[59]	Isogenic to BY4742 LYS2+ Mat α; his3Δ1 ura3Δ0 leu2Δ0
FT001	This study	[YL515] sak1Δ::KanMX [pRS313-SAK1-9myc]
FT002	This study	[YL515] sak1Δ::KanMX [pRS313-SAK1-9myc-10Ala]
FT003	This study	[YL515] HTB2:mSCARLET::URA3 SNF1:mneongreen:KanMX sak1Δ:hphNT1
FT004	This study	[FT003] [pRS313-SAK1-9myc wt]
FT005	This study	[FT003] [pRS313-SAK1-9myc-10Ala]
FT006	This study	[FT001] URA3:pSIVu-TPI1p-ACC1reporter-3xGFP-HA-NLS-ADH1ter
FT007	This study	[FT002] URA3:pSIVu-TPI1p-ACC1reporter-3xGFP-HA-NLS-ADH1ter
MC036	This study	[YL515] sak1Δ:kanMX6
MC394	This study	[YL515] sak1Δ::LEU2
MC508	This study	[MC394] [pRS313-SAK1-9myc wt]
MC509	This study	[MC394] [pRS313-SAK1-9myc-10Ala]
MC221	This study	[YL515] SNF1-HA3:KanMX6
MC395	This study	[MC221] sak1Δ::LEU2
MC510	This study	[MC395] [pRS313-SAK1-9myc wt]
MC511	This study	[MC395] [pRS313-SAK1-9myc-10Ala]
MC048	This study	[YL515] tos3Δ:hph
MC056	This study	[MC048] sak1Δ::KanMX
MC057	This study	[MC056] elm1Δ::HIS3MX
MC501	This study	[MC057] [pRS315-SAK1-9myc wt]
MC503	This study	[MC057] [pRS315-SAK1-9myc-10Ala]
PS003	This study	[YL515] HIS3:pSIVh-TPI1p-ACC1reporter-3xGFP-HA-NLS-ADH1ter
MC281	This study	[YL515] snf1Δ::NatNT2
PS004	This study	[MC281] HIS3:pSIVh-TPI1p-ACC1reporter-3xGFP-HA-NLS-ADH1ter
MC294	This study	[YL515] HIS3:pSIVh-TPI1p-ACC1reporter-GFP-HA-ADH1ter
MC492	This study	[MC294] URA3:pSIVu-CYC1p-SV40-NLS-3xmScarlet
MC295	This study	[YL515] HIS3:pSIVh-TPI1p-ACC1reporter-GFP-HA-NLS-ADH1ter
MC493	This study	[MC295] URA3:pSIVu-CYC1p-SV40-NLS-3xmScarlet
MC494	This study	[PS003] URA3:pSIVu-CYC1p-SV40-NLS-3xmScarlet

(*Continued on next page*)

Continued

REAGENT or RESOURCE	SOURCE	IDENTIFIER
Recombinant DNA		
pRS313	*CEN, ARS, ampR, HIS3*	Sikorski et al.[60]
pFT001	pRS313-SAK1-myc9-wt	This study
pFT002	pRS313-SAK1-myc9-10Ala	This study
pRS315	*CEN, ARS, ampR, URA3*	Sikorski et al.[60]
pMC095	pRS316-SAK1-9myc-wt	This study
pMC093	pRS316-SAK1-9myc-10Ala	This study
pRS426	*CEN, ARS, ampR, URA3*	Christianson et al.[61]
pFA6a-LEU2	TEFp-LEU2-TEFt, ampR	Caligaris et al.[62]
pFA6a-URA3	TEFp-URA3-TEFt, ampR	Nicastro et al.[51]
pFA6a-KanMX6	TEFp-KanMX6-TEFt, ampR	Longtine et al.[63]
pFA6a-NatNT2	TEFp-NatNT2-TEFt, ampR	Janke et al.[64]
pFA6a-GFP-HIS3	GFP-ADH1t-TEFp-HIS3-TEFt	Longtine et al.[63]
pFA6a-HA3-KanMX6	HA3-ADH1t-TEFp-KanMX-TEFt	Longtine et al.[63]
pSIVh	HIS3 shortp-TEFp-SpHIS5-TEFt-MCS1-HIS3t	Wosika et al.[65]
pSIVu	URA3p-TEFp-URA3-TEFt-MCS-URA3t	Wosika et al.[65]
pMC058	[pSIVh] TPIp-ACC1reporter-GFP-HA-ADH1ter	This study
pMC059	[pSIVh] TPIp-ACC1reporter-GFP-HA-NLS-ADH1ter	This study
pMC064	[pSIVh] TPIp-ACC1reporter-3xGFP-HA-NLS-ADH1ter	This study
pFT003	[pSIVu] TPIp-ACC1reporter-3xGFP-HA-NLS-ADH1ter	This study
pMC052	[pSIVu] CYC1p-SV40-NLS-3xmScarlet	This study
Software and algorithms		
ImageJ	NIH	https://imagej.nih.gov/ij/
ACDC	Padovani et al.[66]	https://github.com/SchmollerLab/Cell_ACDC
SnapGene Software	SnapGene	https://www.snapgene.com/
OriginPro	OriginLab	https://www.originlab.com/

EXPERIMENTAL MODEL AND STUDY PARTICIPANT DETAILS

S. cerevisiae strains and plasmids used in this study are listed in the key resources table. Standard genetic methods were used for strain construction. Cells were cultured in a minimal medium (6.7 g/L yeast nitrogen base supplemented with 50 mg/L of the required amino acids and bases) containing 2% glucose, or in YPD (1% yeast extract, 2% peptone, 2% glucose), depending on the experimental setup. For shift-down experiments, cells were pre-cultured in 2% glucose and subsequently transferred to a medium containing either low glucose (0.05%) or 2% ethanol and 3% glycerol, to induce glucose depletion. All cultures were grown at 30°C unless otherwise specified.

METHOD DETAILS

Cytofluorimetric analyses

Cell death was evaluated by propidium iodide (PI) staining at different time points using the Cytoflex cytofluorimeter (Beckman Coulter, Milan, Italy) and analyzed with Cytoflex software (version 2.6.0.105). Protein cell content was measured by fluorescein isothiocianate (FITC) staining as in,[67] analyzed using the Cytoflex cytofluorimeter (Beckman Coulter, Milan, Italy) and quantified with Cytoflex software (version 2.6.0.105).

Live cell imaging microscopy and microfluidics experimental setup

To monitor Snf1 nuclear translocation under metabolic stress conditions, we performed time-lapse imaging using a Leica THUNDER live-cell fluorescence microscope integrated with the CellASIC ONIX2 Microfluidic System. This system provides precise environmental control, allowing dynamic manipulation of media composition, temperature, and gas conditions during live-cell imaging

(Merck Millipore). For the experiments, yeast cells expressing Snf1-mNeonGreen and histone Htb2-mScarlet (as a nuclear marker) were grown overnight in 2% glucose medium, then diluted the next morning 1:5 into fresh 2% glucose medium, and cultured until 1.5×10^7 cells/mL. Cells were then diluted to a final concentration of 4×10^6 cells/mL, sonicated at low power for 10 s, and 50 μL were loaded into the Y04C-02 microfluidic plate (CellASIC ONIX2 system, Merck). Cells were first perfused with 2% glucose medium for 90 min to establish baseline conditions, ensuring that all observed responses were due to the subsequent metabolic shift rather than pre-existing variability. To induce metabolic stress, cells were exposed to either low glucose (0.05%) or 2% ethanol and 3% glycerol-containing medium. The microfluidic system enabled rapid media exchange, allowing real-time observation of immediate Snf1 responses for up to 90 min. Snf1-mNeonGreen and Htb2-mScarlet fluorescence intensities were tracked every 7 min using single-plane acquisition, with Htb2-mScarlet serving as a nuclear marker to facilitate precise segmentation and quantification of nuclear Snf1 levels. The incubation temperature of the cells during live-cell microscopy was maintained at 30°C.

Quantitative analysis and cell cycle analysis

For quantitative analysis, the Cell-ACDC software, an open-source, user-friendly Python-based framework designed for segmentation, tracking, and cell cycle annotation of live-cell imaging data, was used.[66] To assess Snf1-mNeonGreen localization, nuclear fluorescence intensities were extracted from segmented nuclear regions and normalized to baseline levels (T0) measured during the initial glucose-rich condition prior to the media shift. Phase contrast images were used for whole cell segmentation, while nuclear segmentation was performed using the histone Htb2-mScarlet fluorescence. Cell segmentation was performed automatically using the YeaZ neural network integrated into the Cell-ACDC interface,[68] while nuclear segmentation was conducted using Otsu thresholding. Then, the resulting segmentation masks were manually corrected throughout the entire time course to address errors and ensure high-quality data. Among the extracted parameters, nuclear fluorescence concentration was used for quantitative comparisons across time points and conditions, as it accounts for differences in nuclear size. The concentration was calculated as the ratio between the background-corrected total fluorescence inside the segmented nucleus and the nucleus volume. The nucleus volume was estimated from the 2D segmentation mask as described in.[69] Note that the volume estimation from 2D masks was previously validated for budding yeast cells and, given the similar morphology between the cell and the nucleus, we assume it well approximates the nucleus volume too. To ensure the segmented nuclei and the corresponding cells have the same ID, we used the Cell-ACDC utility "Track sub-cellular objects". This workflow automatically assigns to each nucleus the same ID of the cell whose overlap is the highest and at least 40%. Additional parameters, such as Cell and nucleus ID and time frames, were also collected to enable accurate single-cell tracking and phase-specific analysis. To precisely track Snf1-mNeonGreen nuclear translocation in different cell cycle phases, we used Cell-ACDC's cell cycle analysis to classify cells into G1 and S/G2/M phases based on bud morphology and Htb2-mScarlet nuclear marker, which allowed clear discrimination of anaphase completion. To avoid bias due to heterogeneous metabolic histories, only cells present prior to the shift were included in the analysis. Cells that emerged post-shift were excluded, as they developed entirely under low-glucose conditions and did not experience the transition from high to low glucose. All single-cell experiments were performed in two independent biological replicates. For each replicate, 3 technical replicates were acquired by imaging distinct positions. Typically, up to 70 cells per time point were analyzed (as specified in the figure legends). All quantitative data were analyzed using Microsoft Excel for basic processing, while graphical representations of fluorescence trends over time were generated using OriginPro (OriginLab).

Western blot analysis

For glucose shift-down experiments, yeast strains were grown in a minimal medium containing 2% glucose at 30°C. Cultures were incubated until they reached the mid-logarithmic growth phase at ~0.7 $OD_{600\ nm}$/mL. Subsequently, cells were shifted to a medium containing 0.05% glucose to induce glucose depletion. To harvest cells, 10 mL of cells were transferred to a tube containing trichloroacetic acid (TCA) at 6% final concentration. Then cells were washed with ice-cold acetone to remove excess TCA, air-dried, and stored at −80°C until use. For protein extraction, the dried pellets were resuspended in urea buffer (8 M urea, 100 mM Tris-HCl, pH 8.5, and 1% SDS) and disrupted with glass beads on a vortex (as in Caligaris et al., 2023).[35] SDS sample buffer (350 mM Tris-HCl pH 6.8, 10% SDS, 30% glycerol, 0.0002% bromophenol blue, and 600 mM DTT) was then added, and the samples were boiled at 95°C for 5 min to denature the proteins. Protein samples were separated by SDS-PAGE and transferred to nitrocellulose membranes. After the transfer, the membranes were blocked with 5% non-fat dry milk in TBS-T (20 mM Tris-HCl pH 7.4, 150 mM NaCl, 2.7 mM KCl, 0.1% Tween 20) to prevent non-specific binding. Primary antibodies were used to detect key proteins. Conjugated secondary antibodies were applied, and the signal was detected using enhanced chemiluminescence (ECL). The resulting signals were captured using chemiluminescence and Vilber Fusion FX imaging system or Chemidoc system (Bio-Rad). When necessary, membranes were stripped with 0.2 M Gly, 0.5 M NaCl, pH 2.8, and reprobed with other antibodies. The intensity of protein bands was quantified using ImageJ software or ImageLab software, and the values were normalized to total protein levels, as specified in figure legends. Western blots were performed at least in triplicate to ensure reproducibility, and the data were presented as mean values with standard deviations.

ACC1-3xGFP-NLS reporter assay

The ACC1-GFP versions were created from the ACC1-GFP previously described by Deroover et al., 2016[36] and subcloned into pSIVh plasmids.[62] The pSIVh plasmid allows single integration into the *HIS3* locus of the yeast genome. The ACC1-GFP and ACC1-GFP-NLS variants were ordered from GenScript, already subcloned into a pSIVh plasmid. Two extra GFPs were subcloned into the ACC1-GFP-NLS plasmid, via the Gibson Assembly cloning kit (New England Biolabs), to generate the ACC1-3xGFP-NLS variant.

To monitor the nuclear activity of Snf1, yeast cells expressing ACC1-3xGFP-NLS in either WT or *sak1*^{10Ala} cells were initially grown in YPD and subsequently shifted to low glucose. Samples from wild-type and *sak1*^{10Ala} cells were processed in parallel throughout the entire experiment. Before the shift, cells were washed directly on the filter to remove residual glucose. Cells were collected at various time points following the glucose shift-down (0, 5, 10, 15, 20, and 30 min). Protein extracts were prepared and subjected to western blot analysis to detect ACC1-pS79 levels. The phosphorylation signal was normalized to the GFP level to account for protein loading variations. At least three biological replicates were performed to ensure reproducibility, and the data were presented as mean values with standard deviations.

Co-immunoprecipitation (Co-IP) assay

Yeast strains expressing *SNF1-HA*$_3$ and *SAK1-myc*$_9$ variants were pre-grown overnight in a selective medium. The following morning, cells were diluted in 1 L of selective medium to an initial $OD_{600\ nm}$/mL of 0.15. When cells reached a concentration of 1.0 $OD_{600\ nm}$/mL, 500 mL of cells were harvested by filtration and frozen in liquid nitrogen. In parallel, 500 mL of cells were shifted by filtration to a low glucose medium for 30 min. Cells were harvested by filtration and frozen dry ice. Samples from both conditions were processed in parallel through all subsequent steps. Cells were cryogenically disrupted in 4 mL of lysis buffer (50 mM Tris-HCl pH 7.5, 150 mM NaCl, 0.1% NP-40, 10% glycerol, Roche PhoSTOP phosphatase inhibitor, and Roche complete protease inhibitor EDTA-free) in the presence of acid-washed glass beads. Cells were disrupted with cycles of 60 s each, followed by a 60-s interval pause. Protein concentration was measured with the Bradford method.[70] An input aliquot of equilibrated clear lysates was collected and denatured in the presence of SDS sample buffer (350 mM Tris-HCl pH 6.8, 10% SDS, 30% glycerol, 0.0002% bromophenol blue, and 600 mM DTT) for 5 min at 95°C. Clear lysates (3.5 mg) were incubated for 4 h at 4°C with anti-HA affinity matrix (Roche). After 5 washes with lysis buffer, beads were resuspended in 20 μL lysis buffer and denatured in the presence of SDS sample buffer for 5 min at 95°C. Inputs (50 μg) and Co-IPs were analyzed by SDS-PAGE western blot with mouse anti-myc (Cell Signaling, 9B11, 1:1,000 in TBS, 5% milk) and mouse anti-HA (Roche, 12CA5, 1:1,000 in TBS, 5% milk) antibodies. The resulting signals were captured using a chemiluminescence Chemidoc (Bio-Rad) system.

QUANTIFICATION AND STATISTICAL ANALYSIS

To determine statistical significance, we conducted at least two independent biological replicates for each experiment. Data were normalized and then compared using an unpaired Student's *t* test. A *p*-value of less than 0.05 indicated a statistically significant difference between samples. For single cell imaging experiments, nuclear fluorescence intensities were quantified on a per-cell basis using automated segmentation. For each biological replicate, fluorescence values from individual cells were averaged. Details regarding the number of independent replicates, measures of variability, specific statistical tests utilized, and significance criteria are provided in the respective figure legends.